January 2021

Integrative Genomics Implicates Disruption Of Prenatal Neurogenesis In Congenital Hydrocephalus

Shreyas Panchagnula

Integrative genomics implicates disruption of prenatal neurogenesis in congenital hydrocephalus

A Thesis Submitted to

the Yale University School of Medicine

in Partial Fulfillment of the Requirement for

the Joint Degree of Doctor of Medicine (MD)

and Master of Health Science (MHS)

By

Shreyas Panchagnula

2021

I. Abstract

INTEGRATIVE GENOMICS IMPLICATES DISRUPTION OF PRENATAL NEUROGENESIS IN CONGENITAL HYDROCEPHALUS

Shreyas Panchagnula and Kristopher T. Kahle. Section of Pediatric Neurosurgery, Department of Neurosurgery, Yale University, School of Medicine, New Haven, CT.

Congenital Hydrocephalus (CH) affects 1/1000 live births and costs the US healthcare system over $2 billion annually. Mainstay therapies, hinging on surgical cerebrospinal fluid diversion, exhibit high failure rates and substantial morbidity. Limited understanding of pathogenesis warrants identification of crucial genetic drivers underlying CH and their impact on brain development. This pioneering study integrates gene discovery from the largest whole-exome sequenced CH cohort with transcriptional networks (modules) and cell-type markers from the latest transcriptomic atlases of the mid-gestational human brain to uncover the genomic and molecular architecture of CH. Exome analysis of 381 radiographically-confirmed, neurosurgically-treated sporadic CH probands (including 232 case-parent trios) identified genes with rare de novo or transmitted mutations conferring disease risk. Transcriptome analyses identified mid-gestational brain modules and cell-types enriched for cohort-determined CH risk genes, known genes previously implicated in isolated and syndromic forms of CH, and risk genes of Autism Spectrum Disorder (ASD) and Developmental Disorder (DD). Genetic drivers of CH converge in a neurodevelopmental network and in early neurogenic cell-types, implicating genetic disruption of early brain development as a primary patho-mechanism for a significant

subset of CH patients. Genetic and transcriptional overlap with ASD and DD may explain persistence of these conditions in CH patients despite surgical intervention, while greater potency of CH-enriched neural precursors may account for increased frequency of structural brain abnormalities in CH than in ASD or DD alone.

II. Acknowledgements

I would first and foremost like to express my deepest gratitude to my thesis advisor, Dr. Kristopher T. Kahle, for his kindness, his mentorship, and his wholehearted support to my endeavors. Thank you for being my guide and inspiration to pursue scientific investigation and a neurosurgical career.

I would like to thank my thesis department chair, Dr. Angeliki Louvi, and committee member, Dr. Charles Greer, for their mentorship, guidance, and constant support. I am also grateful for the support of my chair, Dr. Murat Günel, and other faculty mentors from the Yale Neurosurgery Department, including Dr. Charles C. Duncan, Michael L. J. Apuzzo, and Michael L. DiLuna. I would like to extend my gratitude to the principal investigators whose collaboration was central to the fulfillment of this project, including Dr. Richard P. Lifton and Dr. Daniel H. Geschwind.

This work would not have been possible without funding support from the Gershon Medical Student Research Fellowship nor without the guidance of the Yale School of Medicine Office of Student Research (OSR). I would like to share my heartfelt thanks to the OSR staff – Dr. John N. Forrest, Dr. Erica Herzog, Dr. Sarwat Chaudhry, Donna Carranzo, Mae Geter, and Kelly Jo Carlson – who worked hard to create a comfortable atmosphere to foster scientific inquiry in medicine.

Thank you to the members of the Kahle Lab – Carol Nelson-Williams, Daniel Duran, Charuta Furey, Jason Karimy, August Allocco, Jonathan Gaillard, Adam Kundishora, Stephanie Robert, Hannah Smith, Ashley Dunbar, Sierra Conine, Phan Q. Duy, Tyrone DeSpenza, Benjamin Reeves, and Arnaud Marlier – who offered both their vital contributions to this project and their invaluable friendships. I am privileged to work in your team. Thank you to the members of the Lifton Lab – Dr. Peter Jin, Dr. Weilai Dong, and Dr. Xue Zeng for their invaluable support. Thank you to Dr. Rebecca L. Walker from the Geschwind Lab for your expertise and unwavering support.

This work is made possible by the members of the Hydrocephalus Association and the hundreds of families affected by hydrocephalus that participated in this study. Thank you for sharing your stories and contributing to research that will hopefully advance our understanding and improve management of this condition.

Thank you to my parents, Ms. Suguna Lanka and Mr. Madhu Panchagnula, and my grandparents, Ms. Prasuna Lanka and Mr. Nageswara Sarma, for believing in me and teaching me to believe in myself via your love, encouragement, and warm presence. Thank you to my ever-increasing circle of family and friends for sharing my struggles and joys.

I’d like to offer my obeisance to the Divine Lord, who pervades the gross universe and that which is beyond, who manifests age after age to demonstrate His infinite mercy, grace, and compassion, and who carves the path and the goal for the mind and the soul.

III. Table of Contents

IV. An Introduction to Congenital Hydrocephalus

Hydrocephalus is the most common disease seen in pediatric neurosurgical practices[1], with a prevalence of roughly 1.1 per 1000 births[2] and a cost of $2 billion to the US healthcare system alone[3]. Hydrocephalus is classically defined as the active, progressive distension of the cerebral ventricular system (i.e. ventriculomegaly) resulting from the inadequate passage of cerebrospinal fluid (CSF) from its main site of production at the choroid plexus epithelium (CPe) to its site of reabsorption into the systemic circulation (e.g. the arachnoid granulations).[4-8] The standard classification scheme of hydrocephalus rests on two fundamental features: etiology, and the anatomy of the CSF conduit.[1,8-11] Hydrocephalus can be acquired (secondary) or congenital (primary) based on the presence or absence of a known etiological antecedent, respectively. The most common forms of secondary hydrocephalus include post-hemorrhagic hydrocephalus (PHH) and postinfectious hydrocephalus.[1,8,11-13] Hydrocephalus can also be non-communicating or communicating based on the presence or absence of obstruction to CSF flow, respectively.[1] Here I review congenital hydrocephalus, including the relevant anatomy and physiology of the developing brain, pathophysiology, clinical features, etiologies, and genetic mechanisms.

Anatomy and Physiology of the Developing Brain Parenchyma and Ventricular System

The pathogenesis of hydrocephalus coincides with key processes pertaining to the development of the brain. Here I will describe some of these neurodevelopmental processes of the brain parenchyma and the ventricular system.

Neural development begins when the notochord induces the ectoderm to differentiate into the neural plate. Through the process of neurulation, the neural plate folds and fuses to form the neural tube. The development of the neural tube creates a lumen that becomes the ventricular system, which encloses CSF and is surrounded by brain parenchymal tissue.[14] At the interface of the ventricular system and brain parenchyma lies a special layer termed the neuroepithelium.[15] This pseudostratified epithelium contains self-renewing neuro-epithelial cells studded with punctate and tight adhesion junctions and demonstrates selective permeability.[16] Owing to myosin regulation, the stretchy neuroepithelium demonstrates elasticity and relaxation to accommodate shaping and expansion of the ventricular cavities.[17]

Two germinal zones arise from the neuroepithelium lining the ventricular wall: the ventricular zone (VZ), and the subventricular zone (SVZ).[14,18-21] The VZ contains neuro-epithelial cells that differentiate into self-renewing multipotent neural stem cells[14], while the SVZ contains neural progenitors that originate from neural stem cells in the VZ[19]. In human brain development, the period of 12 to 18 gestational weeks marks important processes of neurogenesis, including neural proliferation and migration of nascent neurons from the germinal zones to the outer cortex of the developing brain.[22]

In the early ventricular system, CSF is first produced primarily by the neuroepithelium[15], evident from neuroepithelial CSF production studies in several model organisms[23-25], and consistent with the presence of CSF in human brain ventricles ~3-4 weeks before the maturation of a set of specialized vascularized epithelial sheets called the choroid plexus[26]. From the sixth week of gestation, the choroid plexus becomes the main site of CSF production.[7] The bulk flow model explains the conduit of CSF flow from its

origin in the choroid plexus to its absorption in the arachnoid granulations.[27] CSF flow starts in the lateral ventricles and continues through the foramina of Monro into the third ventricle, and then through the cerebral aqueduct into the fourth ventricle. CSF exits the ventricular system via the foramina of Luschka and the medial aperture of the foramina of Magendie into the cisterna magna. When CSF reaches the cortico-subarachnoid spaces and the spinal subarachnoid space, it gets absorbed by arachnoid granulations and drains into the venous sinuses, with small amounts of CSF being absorbed by spinal nerve roots.[7] According to the bulk flow model, the balance of CSF secretion and reabsorption establishes homeostasis in the ventricular system.

The function of CSF hinges on three important properties: osmolarity, pressure, and flow.[15,28] Osmolarity is established by the high rates of ion and water transport in the ventricular system.[1,29,30] Osmolarity gradients established by ion pumps and macromolecule secretion drive continual CSF production facilitated by passive water channels in secretory epithelia.[31-33] Enzymes and ion transport molecules critical to this process include carbonic anhydrase, the bumetanide-sensitive Na-K-2Cl cotransporter NKCC1, and aquaporin (AQP) water channels present in both the choroid plexus and ventricular ependymal cells.[34-37] Changes in CSF osmolarity affect CSF volume and pressure, which are transduced by neuroepithelial mechanosensors and can significantly damage brain parenchymal tissue. CSF flow is key to the distribution of molecular signals and regulatory factors in the CNS.[15]

CSF flow and ciliary function are intertwined in the ventricular system. Two types of cilia adorn the ventricular system: primary nonmotile cilia in monociliated cells, and motile cilia on multiciliated cells.[38] Primary cilia, which can be found on embryonic and

adult neural progenitors[15], function as sensory antennae to facilitate many signaling pathways, including sonic hedgehog (SHH), Wnt, and PDGFR-α pathways.[39-42] These cilia also function as mechanosensors with the ability to detect the directional flow of CSF, transmitting signals to neural progenitors.[43] Thus, monocilia allow cells to respond to developmental cues at several sites of neurogenesis in the CNS and are required for the normal development of neural progenitors. Motile cilia on multiciliated cells generate fluid flow from whip-like beating and are classically thought to facilitate CSF flow.[44] However, the presence of CSF flow prior to the formation of motile cilia in zebrafish suggests that motile cilia may not be essential to CSF flow in embryonic stages.[45]

Pathophysiology of Hydrocephalus

Hydrocephalus is classically explained by the bulk flow model, which implies imbalance in CSF homeostasis as the root pathogenic cause for ventricular distention.[1,46] This homeostatic mechanism of an increase in CSF production relative to CSF reabsorption can manifest in two ways: (1) hypersecretion from the choroid plexus, or (2) obstruction to CSF flow at any point in the CSF conduit from the origin in the choroid plexus epithelium to the most distal point of absorption in the arachnoid granulations. Obstructive and hypersecretory mechanisms of hydrocephalus, often associated with high intracranial pressures (ICPs), are more common in secondary forms of hydrocephalus, especially when they arise from brain hemorrhage, tumor, or infection.[6]

Certain observations of hydrocephalus are inconsistent with the bulk flow model: 1) While congenital forms of hydrocephalus can present with high ICPs, others can have documented ICPs in the borderline-high, normal or even low range and can be associated with severe thinning of the cortical mantle;[1] 2) Functional arachnoid granulations are not

present in children younger than 2 years;[47,48] 3) CSF production is not restricted to the choroid plexus and can come from other ventricular sites;[49] 4) Experimental hydrocephalus can be induced by increasing intraventricular CSF osmolality;[50] and 5) Hydrocephalus can also occur with increased in intraventricular fluid pulsation amplitudes alone without changes in flow or mean CSF pressures.[51-53]

An alternate hydrodynamic model involving intracranial pulsations has been proposed to address some of the inconsistencies with the bulk flow model.[52,54] Clearance of CSF has been shown to not only rely on unidirectional CSF flow but also on cardiac pulsatile movements. These pulsations direct CSF through the foramen magnum into the spinal arachnoid space and back into the skull into the brain parenchyma.[55] In this model, arterial systolic pressure waves in the brain are normally dissipated by subarachnoid spaces, venous capacitance vessels, and intraventricular pulsations transmitted by the choroid plexus. Intraventricular pulsations are absorbed through the ventricular outlet foramina. Dysfunction of pulsation absorbers leads to abnormally high pulsation amplitude, resulting in ventricular expansion.[1] Perturbations in pulsatile movements have been observed in human and murine models of hydrocephalus, but it is debated whether these perturbations are a cause or consequence of hydrocephalus.[56]

Clinical Features of Hydrocephalus

Hydrocephalus can be diagnosed by prenatal ultrasound, as early as 18 to 20 gestational weeks.[57] Detection of ventriculomegaly via ultrasound is often followed by studies such as a higher-level ultrasound scan, fetal MRI, TORCH screen (toxoplasmosis, rubella, cytomegalovirus, herpes simplex), or amniocentesis.[58] Chorionic villus sampling or amniocentesis in known maternal carriers of *L1CAM* can diagnose X-linked

hydrocephalus.[58] Hydrocephalus in infants manifests as abnormally increasing head circumference, irritability, vomiting, bulging of anterior fontanelle, and splaying of cranial sutures. In older children and adults, hydrocephalus can present with headache, vomiting, loss of developmental milestones, diplopia, and papilledema.

Imaging remains the most important diagnostic tool and entails cranial ultrasonography (used to screen for ventriculomegaly patients with an open fontanel), MRI (used to map the anatomy and cause), and cine MRI CSF flow (used to track patient specific changes in CSF hydrodynamics).[59-61]

Current Treatments

Current mainstay therapies include surgical methods of CSF diversion, including CSF shunts and endoscopic third ventriculostomies. The most common type of shunt is the ventriculo-peritoneal shunt (VPS) which utilizes silastic tubing that runs subcutaneously from head to abdomen with a valve between the ventricular and distal catheters. Other types of shunts include ventriculo-atrial shunts and ventriculo-pleural shunts. Shunts often involve differential pressure settings or flow-regulating valve mechanisms with antisiphon or gravitational devices to prevent CSF overdrainage from posture related siphoning.[1]

Another method of surgical diversion, the endoscopic third ventriculostomy, was developed in the 1990s for patients with non-communicating hydrocephalus and is now a routine procedure in the management of the condition.[62] The endoscopic third ventriculostomy involves passing in a scope into the frontal horn of the lateral ventricle, then through the foramen of Monro into the third ventricle. An opening made in the floor of the third ventricle opens direct communication into the prepontine cistern. While the ETV proved to be an initial success in many patients, high rates of failure ensued,

especially in infants.[63] Subsequently, choroid plexus cauterization (CPC) was added to ETV in an effort to decrease failure rates and improve efficacy.[64] ETV and CPC was shown to have better results in children younger than one year compared to ETV alone.[64-68]

Complications in the Acute Setting

Shunt failure, often from mechanical obstruction, occurs in 40% of children within the first two years from original placement with continued risk of failure thereafter.[13] The diagnosis of failure lies in imaging evidence such as increased ventricle size compared to baseline and in clinical symptoms such as headache, vomiting, irritability, decreased level of consciousness, and bulging fontanelle with accelerated head growth in infants.

Shunt obstruction is treated with urgent surgery to identify and replace the obstructed component of the shunt, whether it is the proximal catheter, the distal catheter or the valve. In the case of more subtle symptoms such as chronic headache or deteriorating school performance, ICP monitoring can help establish obstruction as a cause. Perioperative mortality is low, while the estimated 30-year shunt-related mortality is 5-10%.[69,70]

Shunts infections can occur at a rate of 5 to 9% per procedure mostly within three months[71-73] and can present with fever, irritability, wound erythema, or symptoms of shock malfunction. A CSF culture from shunts can elucidate the pathogen. Infection can also present within abdominal system from a peritoneal CSF pseudocyst.[74] In cases of infection, systematic prophylactic antibiotics as well as standardized surgical protocols are utilized for management.[72,75] Another complication for shunts includes overdrainage, which can present with subdural hygroma or hematoma.[76] In these cases, slit-like syndrome develops with a ventricle size of small and accompanies low pressure headaches for acute

intermittent symptoms of shunt obstruction. Treatment schemes may include shunt revision to reduce CSF drainage, shunting lumbar CSF space, and cranial vault expansion.

ETV failure generally occurs at an incidence of about 35%.[77] However, success is dependent on individual prognostic factors including aging cause of hydrocephalus.[63] In this regard it is quantified by the ETV success score.[63,78] Most failures occur within the first six months of surgery[63,79,80], but the failure rate relative to shunts decreases after 2-3 years.[77] Other rare complications include basilar artery injury, permanent endocrinopathy, hypothalamic injury or other brain injury, and perioperative mortality.[81]

Clinical Outcomes in the Long-Term

The degree of long-term cognitive dysfunction in hydrocephalus is linked to the brain dysmorphology or primary injury associated with the causal mechanisms of the disorder. Hydrocephalus is accompanied by impairment in overall intelligence, verbal IQ, spatial navigation, executive function, learning, memory, and processing speed.[82-87] In 20% of patients, a near-normal quality of life is maintained[88]; however other children have significant impediments to quality of life. Epilepsy develops in as many as 34% of patients treated with shunting in infancy.[89] Headaches are frequently reported in shunted hydrocephalus, with 10-20% reporting severe headaches in children[88], and 40% reporting chronic headaches in adults[90]. Depression treatment was reported in 45% of patients, care dependence in 43%, and unemployment in 43%.[91]

Etiologies of Hydrocephalus

Here I will characterize broad categories of the etiologies of human hydrocephalus including structural causes, inflammatory processes, vascular dysfunction, and dysregulated iron and water transport.

Structural causes

Hydrocephalus can arise from structural brain conditions in patients, including myelomeningocele, Chiari II malformation, Dandy-Walker complex, and encephalocele. These syndromes can often entail ependymal denudation and subcommisural organ dysfunction leading to closure of the fetal aqueduct.[92] Mass lesions can also obstruct CSF pathways at the cerebral aqueduct or fourth ventricle. These lesions include developmental cysts and various tumors. Tectal gliomas and other posterior third ventricle tumors can obstruct the aqueduct, while common pediatric posterior fossa brain tumors such as cerebellar astrocytomas, medulloblastomas, and ependymomas can obstruct the outlets of the fourth ventricle.[1]

Inflammatory processes

Infection and hemorrhage can result in inflammation of the meninges or ventricles, inducing hydrocephalus via impairment of CSF circulation and absorption of the normal dampening of arterial pulsations. In developed countries, intraventricular hemorrhage of prematurity is one of the most common causes of acquired hydrocephalus.[13] In Uganda and other sub-Saharan African countries, neonatal ventriculitis with a climate-associated cyclical incidence pattern of infection is a major cause of acquired postinfectious hydrocephalus.[93] Ventricular inflammation induces ependymal scarring, intraventricular obstruction, and multi-compartmental hydrocephalus. In addition, hydrocephalus can arise from the inhibition of ependymal ciliary development and function in fetal ventriculitis, or from blood-borne lysophosphatidic acid on NPC adhesion and localization along the ventricular surface.[94,95]

Vascular dysfunction

Idiopathic venous outflow resistance, venous sinus collapse[96,97], venous thrombosis[98], and venous outlet stenosis at the skull base associated with cranial facial dysostoses such as Crouzon's and Pfeiffer's syndromes[99], are all causes of reduced venous compliance, and can be a primary cause of communicating hydrocephalus. Cerebral hyperaemia has also been documented in cases of idiopathic infant hydrocephalus.[100]

Dysregulated Iron and Water Transport

Aberrant ion and water transport processes in the choroid plexus and ventricular system have been implicated in hydrocephalus.[36,101-104] For example, CSF hypersecretion from choroid plexus hyperplasia and non-obstructive tumors of the choroid plexus have been linked to hydrocephalus.[50] Recently, a recessive genotype in *ATP1A3* encoding the α3 subunit of the Na^+/K^+ ATPase was identified in a human case of hydrocephalus.[105] In addition, mice with knockout of aquaporin water channel AQP4 have been shown to develop obstruction of the aqueduct. [44] Conversely, the upregulation of ependymal AQP4 in late rather than early stages of hydrocephalus suggests a compensatory role for the channel in the maintenance of water homeostasis.[106,107]

Another system that may contribute to the development of hydrocephalus is the glymphatic system, a paravascular system that facilitates water and solute movement from subarachnoid CSF into brain interstitial fluid and out through the deep draining veins.[108,109] Notably, the glymphatic system contains paravascular channels bounded by astrocytic endfeet containing AQP4.[110]

Secondary Effects of Hydrocephalus

The damaging consequences of hydrocephalus lie in the effects of increased ICP and ventriculomegaly. Neurovascular damage and inflammation secondary to increased ICP and ventriculomegaly yield tissue injury that compromises brain development.[92,111] In the acute stage of ventriculomegaly, compression stretch of the periventricular tissue including axons, myelin, and microvessels leads to ischemia, hypoxia, inflammation, and increased CSF pulsatility.[92] The chronic stage of ventriculomegaly entails gliosis, demyelination, axonal degeneration, periventricular edema, metabolic impairments, and changes to the permeability of the blood brain barrier.[92] Hydrocephalus can be exacerbated by ependymal denudation, in which the exposure of the sensitive SVZ to toxic metabolites compromises neurogenesis.[112,113]

Genetic Mechanisms of Congenital Hydrocephalus and the Significance of Next-Generation Sequencing in Neurodevelopmental Disorders

While there is growing evidence of multiple genetic determinants underlying syndromic and non-syndromic forms of hydrocephalus, the genetic and molecular architecture of neurodevelopmental disorders have historically been difficult to study given their complex, highly heritable, and polygenic natures.[114,115] Population studies have revealed familial aggregation of congenital hydrocephalus, increased recurrent risk ratios for same sex twins and first-degree or second-degree relatives.[116,117] Several loci and genes have been linked to non-syndromic forms of CH in animals and syndromic forms of hydrocephalus in humans.[2,7,118,119] Over 100 genes are implicated in these human cases of syndromic hydrocephalus, which entail severe systemic abnormalities (e.g. respiratory, cardiac, and renal) and implicate several biological pathways in the development of hydrocephalus (e.g.

neuronal adhesion, Wnt signaling pathway, vesicle trafficking, dystroglycanopathies, ciliopathies, neural tube defects, planar cell polarity, RASopathies, PIK3-AKT-MTOR pathways, and growth factor signaling).[7] Yet, very few causal mutations have been identified in human non-syndromic hydrocephalus, despite epidemiological studies and reports of familial CH suggesting genetic etiologies for up to 40% of cases.[120] Traditional linkage and targeted sequencing approaches have identified mutations in *L1CAM* (OMIM# 307000), *MPDZ* (OMIM# 615219), *CCDC88C* (OMIM# 236600), and *AP1S2* (OMIM# 300629).[7] The sporadic nature of >95% of CH cases limits the utility of traditional genetic approaches,[7] and the heterogeneity in approaches for gene discovery coupled with the wide range of cellular processes altered by these genes confounds efforts to formulate a uniform paradigm of CH pathophysiology.

In this regard, next-generation sequencing has revolutionized the identification of genetic causes of human disease. Whole exome sequencing (WES) in particular proves to be a powerful unbiased strategy for gene discovery.[5] WES can identify both inherited genetic variants in familial pedigrees and *de novo* mutations (DNMs) in parent-offspring trios.[121] WES of the trio design relies on a simple genetic model, in which the causative mutation of a condition is assumed to be present in the affected child but absent in the unaffected parents. The occurrence of DNMs in the same gene in unrelated individuals implies a potential pathogenic contribution to the disease. Thus, WES of large patient cohorts can identify genes mutated in affected subjects more often than expected by chance.

The advent of next-generation sequencing methods has led to widespread discovery of multiple genetic determinants of neurodevelopmental disorders, including autism[122-124],

craniosynostosis[125], epilepsy[126], brain malformations[127], and other severe, undiagnosed developmental disorders[128]. While these candidate genes provide molecular clues for pathogenesis, locus heterogeneity and biological pleiotropy complicates our ability to predict how these genetic alterations affect the inherently complex biological pathways of brain development.[129]

One solution in translating genetic findings to a higher-level mechanistic insight lies in the identification of pathways that mark convergence of the biological activity of genes conferring high risk for a particular condition. To that end, transcriptomic mapping with RNA-seq allows for the investigation of gene expression patterns in the developing human brain, an approach termed "integrative genomics". Given the likelihood that genetic perturbations involved in a disorder are likely to have converging pathways[129], WES genetic variants are integrated with human transcriptomes to determine points of convergence in developing brain regions, developmental periods, gene co-expression networks, and individual cell types.

In a pioneering study using BrainSpan, a spatio-temporal transcriptomic atlas of the developing human brain (from embryonic to late adulthood stages)[130], ASD-associated variants converge in cortical glutamatergic projection neurons during the midfetal period.[131] Using the same transcriptomic atlas, another study found that ASD-associated genes coalesce in modules, or co-expression networks identified via weighted gene co-expression network analysis (WGCNA).[132] These modules are characterized by distinct biological functions, such as early transcriptional regulation and synaptic development.[133] Importantly, these studies leveraged co-expression networks to construct a spatio-temporal

map of ASD risk gene expression, identifying mid-fetal glutamatergic projection neurons as a point of convergence with potential disease implications.[131,133]

In a recent study, Satterstrom et al. provided further evidence for the role of ASD risk genes in early brain development and excitatory-inhibitory neuron imbalance.[124] By examining risk gene enrichment in a single-cell RNA-seq dataset from prenatal human forebrain[134], this study demonstrated that ASD genes are most strongly enriched in early excitatory neurons and striatal interneurons, thus implicating maturing and mature neurons of both excitatory and inhibitory lineages.[124] Taken together, these studies highlight the power of integrative genomic approaches for elucidating the spatiotemporal dynamics and significance in early brain development of risk genes of a given disorder.

I now present findings from the largest WES study to date of sporadic, neurosurgically-treated CH, integrated with transcriptomics of human brain development.

V. Statement of Purpose

With the purpose of gaining better insight into the pathogenesis of CH, the goal of this study is to elucidate the genetic and molecular architecture of CH through the integration of gene discovery from the largest whole-exome sequenced CH cohort with transcriptional networks (modules) and cell-type markers from the latest transcriptomic atlases of the mid-gestational human brain to uncover the genomic and molecular architecture of CH. Thus, I present my findings from my project with the following specific aims:

Specific Aim 1: Establishing a large and deeply phenotyped CH patient cohort.

In this aim, we will establish a CH patient cohort with an innovative and collaborative social-media recruitment platform. Probands that satisfy our inclusion criteria demonstrate: 1) the diagnosis of primary CH (i.e., not due to secondary or syndromic causes); 2) no documentation of *L1CAM* mutation; and 3) the availability of both biological parents to contribute DNA. Probands are actively recruited from Yale School of Medicine (YSM) and our collaborating institutions (Boston Children's Hospital, USA; CURE Hospital, Uganda; Marmara Hospital, Turkey). We will also employ a unique social media recruitment strategy utilizing Facebook, approved by the Yale University IRB/HIC (Kristopher Kahle, PI; HIC/HSC Protocol#: 1602017144), which allows us to efficiently identify and rapidly obtain DNA from CH patients around the world using mailed consent forms and buccal swab kits. We place emphasis on collecting DNA from children with severe cases of CH that have undergone treatment, and families with multiple affected members. For each index case, we obtain full medical records, prior clinical genetic testing, and importantly, full brain MRIs and neuroradiology reports.

Specific Aim 2: Identification of novel CH-causing genes using whole exome capture and massively parallel DNA sequencing.

In this aim, we will utilize WES and bioinformatics to identify novel CH-causing mutations. All trios are sequenced at the Yale Center for Genome Analysis (YCGA). Resulting sequence is analyzed with computational pipelines that enable the rapid identification of rare/novel/de novo variants which are predicted to alter the function of the encoded protein, are specific for the disease, and are not detected in published and internal reference SNV sequence databases of unaffected patients.[135] Assuming that there are single loci accounting for the majority of remaining heritability, we predict WES will detect several novel CH genes. We predict genes may cluster in pathways relevant for neurodevelopment. We anticipate it will be possible to identify multiple independent mutations in the same genes or genetic pathways in different individuals with similar phenotypes.

Specific Aim 3: Identification of gene co-expression networks and cell types pertinent to CH risk genes from transcriptomic atlases of the developing human brain.

In this aim, we will harness two previously published transcriptomic atlases of the mid-gestational human brain: a bulk RNA-seq atlas characterized by WGCNA modules, and a single cell (sc)RNA-seq atlas characterized by cell type markers. We will test for enrichment of cohort-determined risk genes as well as known syndromic genes of hydrocephalus in these modules and cell type markers to identify biological points of convergence from genotype to phenotype. We will also test the enrichment of risk genes for autism spectrum disorder (ASD) and developmental disorders (DD) for comparison between biological pathways of CH and other neurodevelopmental disorders.

Please note that a subset of the work presented hereafter has been published prior as material from:

Jin SC*, Dong W*, Kundishora AJ*, **Panchagnula S***, Moreno-De-Luca A*, Furey CG, Allocco AA, Walker RL, Nelson-Williams C, Smith H, Dunbar A, Conine S, Lu Q, Zeng X, Sierant MC, Knight JR, Sullivan W, Duy PQ, DeSpenza T, Reeves BC, Karimy JK, Marlier A, Castaldi C, Tikhonova IR, Li B, Peña HP, Broach JR, Kabachelor EM, Ssenyonga P, Hehnly C, Ge L, Keren B, Timberlake AT, Goto J, Mangano FT, Johnston JM, Butler WE, Warf BC, Smith ER, Schiff SJ, Limbrick DD Jr, Heuer G, Jackson EM, Iskandar BJ, Mane S, Haider S, Guclu B, Bayri Y, Sahin Y, Duncan CC, Apuzzo MLJ, DiLuna ML, Hoffman EJ, Sestan N, Ment LR, Alper SL, Bilguvar K, Geschwind DH, Günel M, Lifton RP, Kahle KT. Exome sequencing implicates genetic disruption of prenatal neuro-gliogenesis in sporadic congenital hydrocephalus. Nat Med. 2020 Nov;26(11):1754-1765. doi: 10.1038/s41591-020-1090-2. Epub 2020 Oct 19. PMID: 33077954.

*These authors contributed equally: Sheng Chih Jin, Weilai Dong, Adam J. Kundishora, **Shreyas Panchagnula**, Andres Moreno-De-Luca.

VI. Methods

Patients

All study procedures and protocols comply with Yale University's Human Investigation Committee and Human Research Protection Program. Written informed consent for genetic studies was obtained from all participants. Inclusion criteria included patients with primary CH who did not carry a genetic diagnosis before surgical treatment or inclusion in the study. Subjects with either a known chromosomal aneuploidy or a copy-number variation with known association to CH were also excluded. Hydrocephalus cases with secondarily acquired etiologies such as intraventricular hemorrhage, meningitis or other central nervous system infection, obstruction due to tumors or cysts and stroke were excluded. Children with hydranencephaly, large cysts and cephaloceles, myelomeningocele (Chiari II malformation) or benign extra-axial CSF accumulation (benign external hydrocephalus) were also excluded. Sequenced trios were composed of 381 primary CH probands including 232 parent–offspring trios and 149 singletons (**Supplementary Tables 1 and 2**). All probands had undergone surgery for therapeutic CSF diversion (shunt placement and/or endoscopic third ventriculostomy). Patients and participating family members provided buccal swab samples (Isohelix SK-2S DNA buccal swab kits), medical records, neuroimaging studies, operative reports and CH phenotype data.

Controls consisted of 1,798 unaffected siblings of people with ASD and unaffected parents from SSC.[136] Only the unaffected siblings and parents, as designated by SSC, were included in the analysis and served as controls for this study. Permission to access to the genomic data in the SSC on the National Institute of Mental Health Data Repository was

obtained. Written informed consent for all participants was provided by the Simons Foundation Autism Research Initiative.

Whole-exome sequencing and variant calling

Exon capture was performed on genomic DNA samples derived from saliva or blood using Roche SeqCap EZ MedExome Target Enrichment kit or IDT xGen target capture kit followed by 101 or 148 base-paired-end sequencing on the Illumina platforms as described previously.[137,138] Sequence reads were aligned to the human reference genome GRCh37/hg19 using BWA-MEM. Single-nucleotide variants and small indels were called using a combination of GATK HaplotypeCaller[139,140] and Freebayes[141] and annotated using ANNOVAR[142]. Allele frequencies were annotated in the Exome Aggregation Consortium, gnomAD (v.2.1.1) and Bravo databases.[143,144] MetaSVM and MPC algorithms were used to predict deleteriousness of missense variants (D-Mis, defined as MetaSVM-deleterious or MPC-score ≥2).[145,146] Inferred LoF variants consisted of stop-gain, stop-loss, frameshift insertions/deletions, canonical splice site and start-loss. LoF and D-Mis mutations were considered 'damaging'. PCR amplicons containing the mutation verified mutations in genes of interest.

DNMs were called using TrioDeNovo.[147] Candidate DNMs were further filtered based on the following criteria: (1) exonic or splice-site variants; (2) read depth (DP) of 10 in the proband and both parents; (3) minimum proband alternative read depth of 5; (4) proband alternative allele ratio ≥28% if having <10 alternative reads or ≥20% if having ≥10 alternative reads; (5) alternative allele ratio in both parents ≤3.5%; and (6) global MAF $\leq 4 \times 10^{-4}$ in the Exome Aggregation Consortium database.

For recessive variant analysis, we filtered for rare (MAF $\leq 1 \times 10^{-3}$ in Bravo and in-cohort MAF $\leq 5 \times 10^{-3}$) homozygous and compound heterozygous variants that exhibited high-quality sequence reads (pass GATK variant quality score recalibration, ≥4 total reads total for homozygous and ≥8 reads for compound heterozygous variants, genotype quality (GQ) score ≥10 for homozygous and GQ score ≥20 for compound heterozygous variants). Only LoF, D-Mis and nonframeshift indels were considered potentially damaging to the disease. For probands whose parents' WES data were not available, only homozygous variants were analyzed.

For rare heterozygous variants, only LoF and D-Mis mutations were considered to be potentially disease associated and were filtered using the following criteria: (1) pass GATK variant quality score recalibration; (2) MAF $\leq 5 \times 10^{-5}$ in Bravo and in-cohort MAF $\leq 5 \times 10^{-3}$; (3) DP ≥8 independent reads; and (4) GQ score ≥20. RGs and DNMs were excluded.

After filtering using the aforementioned criteria for each type of mutation, in silico visualization was performed to remove false-positive calls. Variants in the top candidate genes were further confirmed by Sanger sequencing.

Quantification and statistical analysis

DNM expectation model

Because the CH trios were captured by two different reagents (MedExome and IDT), we took the union of all bases covered by different capture reagents and generated a Browser Extensible Data file representing a unified capture for all trios. We used bedtools (v.2.27.1) to extract sequences from the Browser Extensible Data file.[148] We then applied a sequence context-based method to calculate the probability of observing a DNM for each

base in the coding region, adjusting for sequencing depth in each gene as described previously.[149] Briefly, for each base in the exome, the probability of observing every trinucleotide mutating to other trinucleotides was determined. ANNOVAR (v2015Mar22) was used to annotate the consequence of each possible substitution. RefSeq was used to annotate variants (based on the file 'hg19_refGene.txt' provided by ANNOVAR). For each gene, the coding consequence of each potential substitution was summed for each functional class (synonymous, missense, canonical splice site, frameshift insertions/deletions, stop-gain, stop-loss and start-lost) to determine gene-specific mutation probabilities.[149] The probability of a frameshift mutation was determined by multiplying the probability of a stop-gain mutation by 1.25, as described previously.[149] In-frame insertions or deletions are not accounted for by the model and were not considered in the downstream statistical analyses. To align with ANNOVAR annotations, analysis was limited to variants that were located in the exonic or canonical splice site regions and were not annotated as 'unknown' by ANNOVAR. Following the inclusion criteria, we identified potential coding mutations and generated gene-specific mutation probabilities for 19,347 unique genes. Owing to the difference in exome capture kits, DNA sequencing platforms and variable sequencing coverage between case and control cohorts, separate de novo probability tables were generated for cases and controls, respectively.

Estimation of expected number of rare transmitted variants

We implemented a multivariate regression model to quantify the enrichment of rare transmitted variants in a specific gene or gene set in cases, independent of controls. Additional details about the modeling of the distribution of recessive and transmitted heterozygous variant counts are described in our recent study.[150]

De novo enrichment analysis

The burden of DNMs in CH cases and unaffected ASD controls was determined using the denovolyzeR package[151] as previously described[150]. Briefly, the expected number of DNMs in case and control cohorts across each functional class was calculated by taking the sum of each functional class-specific probability multiplied by the number of probands in the study 2× (diploid genomes). Then, the expected number of DNMs across functional classes was compared to the observed number in each study using a one-tailed Poisson test.[149] Gene set enrichment analyses only considered mutations observed or expected in genes within the specified gene set (high brain-expressed, LoF-intolerant).

To examine whether any individual gene contains more protein-altering DNMs than expected, the expected number of protein-altering DNMs was calculated from the corresponding probability adjusting for cohort size. A one-tailed Poisson test was then used to compare the observed DNMs for each gene versus expected. As separate tests were performed for protein-altering, protein-damaging and LoF DNMs, the Bonferroni multiple-testing threshold is, therefore, equal to 8.6×10^{-7} (= 0.05 / (3 tests × 19,347 genes)).

To estimate the number of genes with multiple DNMs, one million permutations were performed to derive the empirical distribution of the number of genes with multiple DNMs. For each permutation, the number of DNMs observed in each functional class was randomly distributed across the genome adjusting for gene mutability. The empirical *p-value* was calculated as the proportion of times that the number of recurrent genes from the permutation equals or exceeds the observed number of recurrent genes as follows:

$$Empirical\ p-value = \frac{\sum_{i=1}^{1M} I(P_i \geq M)}{1{,}000{,}000}$$

Enrichment analysis for dominant and recessive variants

We implemented a polynomial regression model coupled with a one-tailed binomial test to quantify the enrichment of damaging RGs in a specific gene or gene set in cases and controls, separately as described previously.[150] The expectation of the RG count for each gene was calculated by the formula below:

$$\text{Expected RG}_i = \text{N} \times \frac{\text{Fitted value}_i}{\sum_{Genes} \text{Fitted value}}$$

where 'i' denotes the 'ith' gene and 'N' denotes the total number of RGs. For a given gene set, the expected RG count was based on the sum of fitted values for the gene set.

$$\text{Expected RG}_{Gene\ Set} = N \times \frac{\sum_{Gene\ Set} \text{Fitted value}}{\sum_{Genes} \text{Fitted value}}$$

For rare damaging or LoF heterozygous variants, we found that the number of damaging or LoF heterozygous variants in a gene was inversely correlated with the pLI score obtained from the gnomAD database. To control for the potential confounding effect due to the pLI score, we stratified genes into five subsets by pLI quartiles: (i) those with a pLI score between 0 and the first quantile (6.4×10^{-8}); (ii) those with a pLI score between the first quantile and the second quantile (pLI = 1.9×10^{-3}); (iii) those with a pLI score between the second quantile and the third quantile (pLI = 0.48); (iv) those with a pLI score between third quantile and 1; (v) those without a pLI score. For each set, the expected number of damaging or LoF heterozygous variants for a gene was estimated by the following formula:

$$\text{Expected heterozygous}_{j,k} = \text{L}_k \times \frac{\text{mutability}_j}{\sum_{set_k} \text{mutability}_j}$$

where ‘j’ denotes the ‘jth’ gene, ‘k’ denotes the ‘kth’ set, and ‘L’ denotes the total number of damaging or LoF heterozygous variants.

Case–control burden analysis

Case and control cohorts were processed using the same pipeline and filtered with the same criteria. A one-sided Fisher’s exact test was used to compare the observed number of total alternative alleles, regardless of the transmission pattern in cases to controls in the gnomAD (without disease-enriched TOPMed samples) database.

Determining gene lists

The gene lists used for recessive enrichment analysis were curated as below. The mH genes were compiled by the association of their disease model, disease ortholog or phenotype with hydrocephalus per MGI (http://www.informatics.jax.org/). The dystroglycanopathies genes and ciliopathies genes were compiled by Kousi and Katsanis.[7] Cell adhesion molecules, synaptic vesicle cycle, Ras signaling pathway, Wnt signaling, PI3K–ATK–mTOR pathway, and lysosomal storage disorder gene sets were curated based on KEGG and pathway database and the HUGO Gene Nomenclature Committee. A planar cell polarity gene list was curated based on Wang et al.[152] and Tissir and Goffinet[153].

Gene lists from transcriptomic analyses were curated as below. Risk genes from our CH cohort were defined as genes that harbored ≥1 inherited heterozygous LoF mutation of genome-wide significance, genes intolerant to LoF mutations (pLI > 0.9) with ≥1 LoF DNM and genes intolerant to missense mutations (mis-Z > 2) with ≥1 missense DNM. These genes were categorized as high confidence if they harbored ≥1 inherited heterozygous LoF mutation of genome-wide significance or ≥2 protein-altering DNMs; and as probable risk if they harbored 1 protein-altering DNM. This yielded a high

confidence set of 9 hydrocephalus genes (*TRIM71*, *PTEN*, *PIK3CA*, *SMARCC1*, *FMN2*, *MTOR*, *FOXJ1*, *PTCH1* and *FXYD2*) and a probable set of 55 genes.

We assembled lists of genes previously known to cause isolated and syndromic forms of hydrocephalus in humans from three publications: Kousi and Katsanis summarized over 100 genes described in known hydrocephalus syndromes[7], Furey et. al. outlined new genes implicated in CH through WES[137], and Shaheen et. al. summarized genes with recessive mutations linked to familial forms of CH[154].

We compiled a list of genes with rare risk variation in ASD from two papers: Ruzzo et. al.[123], which describes genes harboring rare inherited variants and Satterstrom et. al.[124], which describes genes with de novo variants and case–control variation. We compiled a list of developmental disorder (DD) risk genes from DDD 2017[128], which describes genes enriched in damaging DNMs.

Module enrichment

Module gene lists were obtained from a bulk RNA-seq atlas from of the midgestational human prenatal cortex (14–21 gestational weeks).[155] WGCNA[156] of this atlas identified modules (labeled by color) of genes that share highly similar expression patterns during midgestational cortical development.[155] In a background set of all genes categorized in coexpression modules, we used a logistic regression for an indicator-based enrichment: $\text{is.disease} \sim \text{is.module} + \text{gene covariates}$ (GC content, gene length and mean expression in bulk RNA-seq atlas), as described previously.[155] Of the 18 WGCNA modules, the gray module, by WGCNA convention[157], contains all genes that do not coexpress and are consequently unassigned to a coexpression network. Thus, the gray

module was excluded from enrichment testing and enrichment significance was defined at the Bonferroni multiple-testing cutoff ($\alpha = 0.05 / 17 = 2.94 \times 10^{-3}$).

Module GO and HP profiling

We used g:GOSt from g:Profiler, a tool for functional profiling of gene lists, to obtain descriptive terms for enriched modules.[158] We used all annotated genes as the statistical domain scope, the g:SCS algorithm to address multiple testing and P = 0.05 as a user-defined threshold for statistical significance. For each gene list, we retained terms of 100–1,000 genes and we plotted the top 20 enriched terms from GO biological process annotations and the top 20 enriched terms from HP ontology annotations.

Cell type enrichment

Cell-type-enriched genes (cell type markers), were obtained from a scRNA-seq atlas that maps the human midgestational cortex (17–18 gestational weeks).[159] In a background set of all genes expressed in ≥3 cells of the scRNA-seq atlas, we used a logistic regression for indicator-based enrichment: is.cell.type ~ is.disease + gene covariates (GC content, gene length). Enrichment significance was defined at the Bonferroni multiple-testing cutoff ($\alpha = 0.05 / 16 = 3.13 \times 10^{-3}$).

Overlap analysis

As described previously[150], permutation test was performed to assess the enrichment of overlapping genes with either damaging (D-mis + LoF) or LoF DNMs shared between CH and four other trio-based cohorts: autism, developmental disorder, idiopathic cerebral palsy, and congenital heart disease. Given the observed numbers of genes with DNMs in the CH and other cohorts as N_1 and N_2, respectively, and the observed number of overlapping genes as M, we sampled N_1 genes from all genes in the CH cohort

and N_2 genes from all genes in the autism cohorts without replacement using the probability of observing at least one DNM as weight. The number of overlapping genes, P, was determined in each interaction of the simulation. A total of 1,000,000 iterations were conducted to construct the empirical distribution. The empirical number of overlapping genes was calculated by taking the average of the number of overlapping genes across all iterations. The empirical P value was calculated as follows:

$$Empirical\ P\ value = \frac{\sum_{i=1}^{1M} I(P_i \geq M)}{1{,}000{,}000}$$

Attribution of Work

Shreyas Panchagnula conceived, designed, and directed the integrative genomic and transcriptomic analyses of the study. Transcriptomic data was provided by Rebecca L. Walker from Dr. Daniel H. Geschwind's lab.

Dr. Kristopher T. Kahle posted to social media site information pertaining to the genetics study and potential participants reached out by email. The management of the secure Yale email address; recruitment of subjects to the genetics study; acquisition of consent, information, cheek swabs; and deep clinical and neuroradiographic phenotyping was a collective effort of the Kahle lab, including **Shreyas Panchagnula**, Dr. Adam J. Kundishora, Dr. Charuta G. Furey, August A. Allocco, Hannah Smith, Ashley Dunbar, Sierra Conine, William Sullivan, Phan Q. Duy, Tyrone DeSpenza, Benjamin C. Reeves, Jason K. Karimy, and Andrew T. Timberlake. Participant information was stored in a HIPAA compliant manner in a RedCap database. DNA was extracted from cheek swabs by Carol Nelson-Williams. Exome analysis was performed by Dr. Peter Jin, Dr. Weilai Dong, and Dr. Xue Zheng from Dr. Richard P. Lifton's lab, to select candidate genes with input from Dr. Kahle. Manuscript and figures were prepared by Dr. Peter Jin, Dr. Weilai

Dong, Dr. Adam J. Kundishora, **Shreyas Panchagnula**, Dr. Andres Moreno-De-Luca, and Dr. Arnaud T. Marlier.

Our Yale based collaborators, including Michael L. DiLuna and Murat Gunel, referred cases seen at Yale. The many members of the Kahle, Gunel, and Lifton labs including Charuta Furey, August Allocco, Ava Hunt, Sierra Conine, Jason K. Karimy, Qiongshi Lu, Andrew T. Timberlake, and Weilai Dong also contributed their feedback, insights, and assistance with recruitment and genetic analysis.

VII. Results

We recruited 381 genetically undiagnosed probands (including 232 parent–offspring trios) with sporadic, neurosurgically treated, primary (developmental) CH (excluding myelomeningocele) (**Supplementary Table 1**), including 169 previously reported CH probands with 125 trios[137]. Studies were Institutional Review Board (IRB)-approved by Yale's Human Research Protection Program (**Methods**). DNA was isolated and WES was performed.[137] A total of 1,798 control trios (comprising unaffected siblings and parents of patients with autism spectrum disorder (ASD) from the Simons Simplex Collection (SSC) cohort) were analyzed in parallel (**Supplementary Tables 2 and 3**). Overall, 8.7% of probands were from consanguineous union, versus 1.3% ASD sibling controls (**Supplementary Table 2**; **Methods** for sequence variant calling, calibration, annotation and validation). Mutations in known familial CH genes[7] accounted for ~2.1% of cases, including mutations in *L1CAM* (OMIM no. 307000), *MPDZ* (OMIM no. 615219), *FLNA* (OMIM no. 300049) and *CRB2* (OMIM no. 219730) described in **Supplementary Table 4**. Removal of the eight patients from further analyses yielded 373 CH probands, including 225 trios.

Protein-damaging de novo mutations account for a large fraction of sporadic CH

The average de novo mutation (DNM) rate of 1.307 per subject resembled previous results with the identical sequencing platform[138] and followed a Poisson distribution (**Supplementary Fig. 1**). Protein-damaging DNMs were significantly enriched among all genes (enrichment of 1.72, $P = 6.6 \times 10^{-7}$; **Supplementary Table 5**), with greater enrichment among genes intolerant of loss-of-function (LoF) mutations ($pLI \geq 0.9$ in gnomAD v.2.1.1) and among genes in the top quartile of mouse brain bulk RNA-

sequencing (RNA-seq) expression (**Methods**). Enrichment was greatest among genes meeting both criteria (3.71-fold, $P = 5.0 \times 10^{-9}$; **Supplementary Table 5**). We estimated that damaging DNMs can account for 17.7% of cases in this cohort (**Supplementary Table 5**).

Twelve genes had ≥2 protein-altering DNMs (**Table 1a**) versus 2.7 genes expected by chance (4.5-fold enrichment; $P = 8.0 \times 10^{-6}$ by 1 million permutations; **Table 1b**). Greater enrichment of recurrent genes was observed in LoF-intolerant genes with multiple DNMs (8.9-fold enrichment; $P = 1.0 \times 10^{-5}$; **Table 1c**), supporting these as causal CH disease genes. Five genes (*TRIM71*, *SMARCC1*, *PTEN*, *PIK3CA* and *FOXJ1*) had significantly more protein-altering DNMs than expected by chance (P value threshold of 8.6×10^{-7} after correction for testing 19,347 RefSeq genes in triplicate using a one-tailed Poisson test; **Table 1a**). Three other genes that are highly intolerant of LoF mutations exhibited ≥2 protein-altering DNMs: *MTOR*, *PTCH1* and *FMN2*. Mutations in these cohort-determined risk genes (*TRIM71*, *SMARCC1*, *PTEN*, *PIK3CA*, *FOXJ1*, *MTOR*, *PTCH1* and *FMN2*) are outlined in **Figures 1-8**.

Table 1: Genes with multiple DNMs are candidate CH risk genes

A. Genes with ≥2 protein-altering DNMs

Gene	# LoF	# D-mis	# T-mis	Poisson P-value	pLI	mis_z
TRIM71	**0**	**6**	**0**	**2.4×10^{-16}**	**1.00**	**3.28**
PTEN	**2**	**1**	**0**	**1.9×10^{-8}**	**0.26**	**3.49**
SMARCC1	**2**	**1**	**0**	**2.0×10^{-8}**	**1.00**	**2.45**
FOXJ1	**2**	**0**	**0**	**1.4×10^{-7}**	**0.97**	**0.70**
PIK3CA	**0**	**1**	**2**	**4.9×10^{-7}**	**1.00**	**5.60**
PTCH1	2	0	0	3.0×10^{-6}	1.00	1.68
PLOD2	0	2	0	1.6×10^{-5}	0.00	0.56
SGSM3	0	0	2	1.0×10^{-4}	0.00	0.16
LRIG1	1	0	1	1.7×10^{-4}	0.04	-1.18
FMN2	1	0	1	4.4×10^{-4}	1.00	0.32
MTOR	0	1	1	9.1×10^{-4}	1.00	7.02
MUC17	0	0	2	1.3×10^{-3}	0.00	-7.83

(A) Twelve genes with more than 1 protein-altering DNMs found in cases. P-values are calculated using the one-tailed Poisson test comparing the observed number of DNMs for each gene versus expected. As separate tests were performed for protein-altering, protein-damaging, and LoF DNMs, the Bonferroni multiple-testing threshold is equal to 8.6x10-7 (=0.05/[3 tests*19,347 genes]). The most significant p-value of the three tests was reported. pLI and mis-z values are based on gnomAD v2.1.1.

B. Genes with multiple DNMs in 225 cases (observed vs expected)

	Observed	Expected	Enrichment	P-value
Syn	0	0.18	0	1
Missense	6	1.86	3.23	0.01
D-mis	2	0.29	7.01	0.03
LoF	4	0.08	48.38	3.0×10^{-6}
Protein-damaging	6	0.85	7.08	1.3×10^{-4}
Protein-altering	12	2.66	4.5	8.0×10^{-6}

(B) More genes with multiple DNMs were detected in 225 case trios than expected by chance, as shown by the observed numbers of genes with > 1 DNM in each variant category. 1 million simulations were performed, based on the per-base probability of mutations in each category, to determine the likelihood and the expected number of genes with > 1 DNM.

C. LoF-intolerant genes with multiple DNMs in 225 cases (observed vs expected)

	Observed	Expected	Enrichment	P-value
Syn	0	0.05	0	1
Missense	3	0.54	5.52	0.02
D-mis	1	0.12	8.2	0.12
LoF	3	0.02	121.02	2.0×10^{-6}
Protein-damaging	4	0.36	11.03	4.5×10^{-4}
Protein-altering	7	0.79	8.9	1.0×10^{-5}

(C) Greater enrichment than expected by chance was observed when restricting analysis to LoF-intolerant genes (N = 3,049) with multiple DNMs in 225 case trios.

D. LoF-tolerant genes with multiple DNMs in 225 cases (observed vs expected)

	Observed	Expected	Enrichment	P-value
Syn	0	0.13	0	1
Missense	3	1.31	2.28	0.14
D-mis	1	0.16	6.12	0.15
LoF	1	0.06	17.27	0.06
Protein-damaging	2	0.48	4.12	0.08
Protein-altering	5	1.88	2.66	0.04

(D) Restricting analysis to genes tolerant to LoF mutations showed marginal enrichment for genes with multiple protein-altering mutations.

D-mis: Damaging missense mutations; T-mis: Tolerated missense mutations; Protein-altering: Missense + LoF; Protein-damaging: D-mis + LoF.

Fig. 1: De novo, transmitted, and unphased mutations in *TRIM71*.

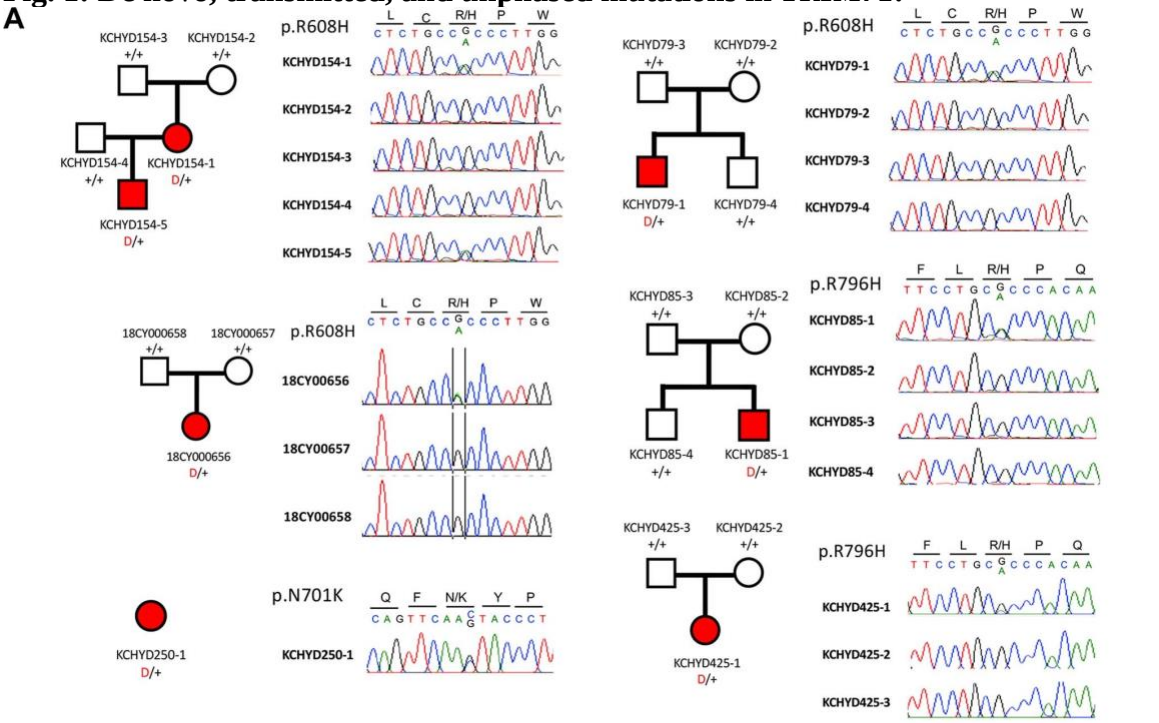

a, Pedigrees and sequencing electropherograms of Sanger sequencing depict all *TRIM71* mutations in genomic DNA from CH probands. **b,** Representative T1 or T2-weighted brain magnetic resonance images for all available probands.

Fig. 2: De novo, transmitted, and unphased mutations in *SMARCC1*.

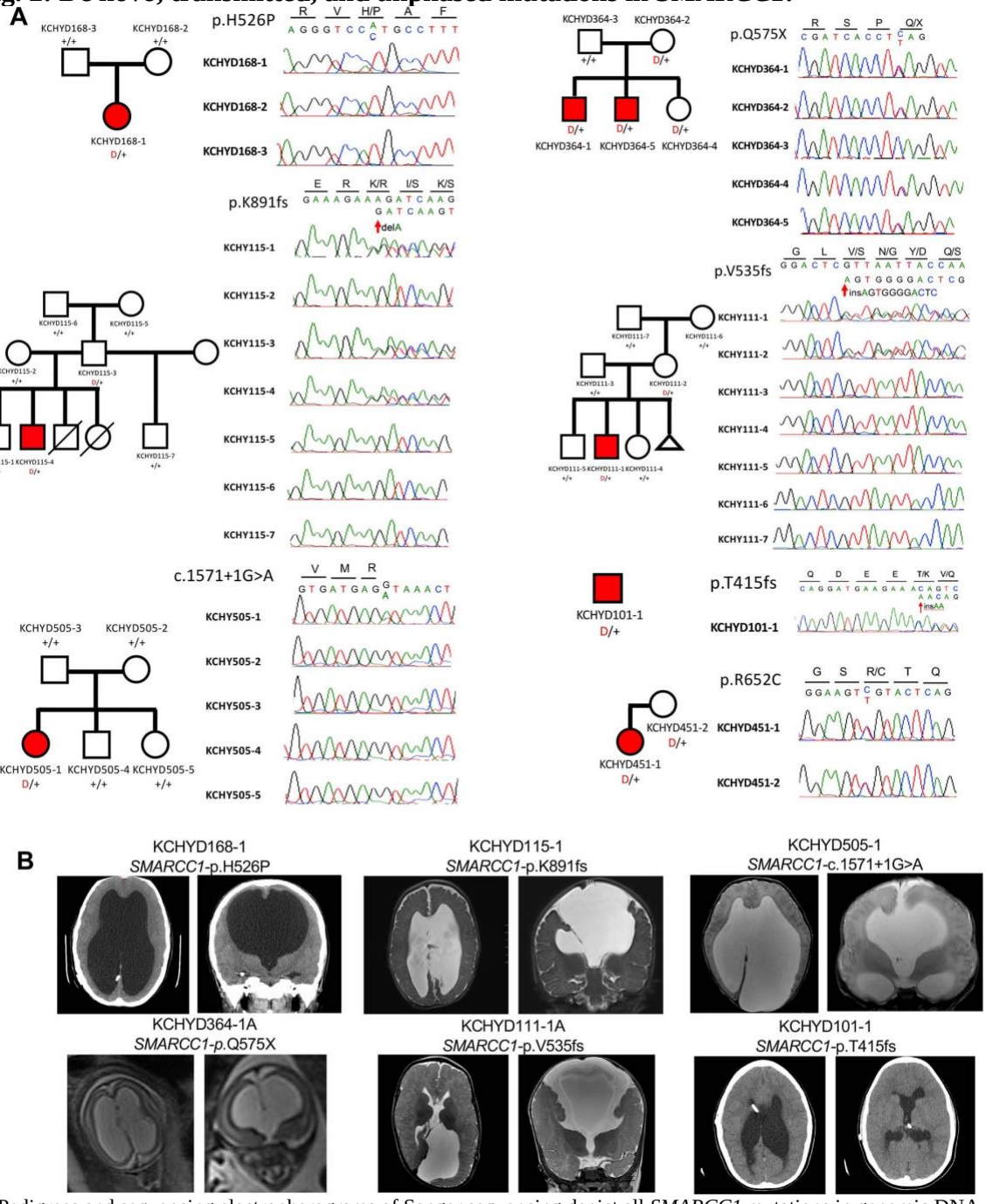

a, Pedigrees and sequencing electropherograms of Sanger sequencing depict all *SMARCC1* mutations in genomic DNA from CH probands. **b,** Representative T1 or T2-weighted brain magnetic resonance images or head CTs for all available probands.

Fig. 3: De novo, transmitted, and unphased mutations in *PIK3CA*.

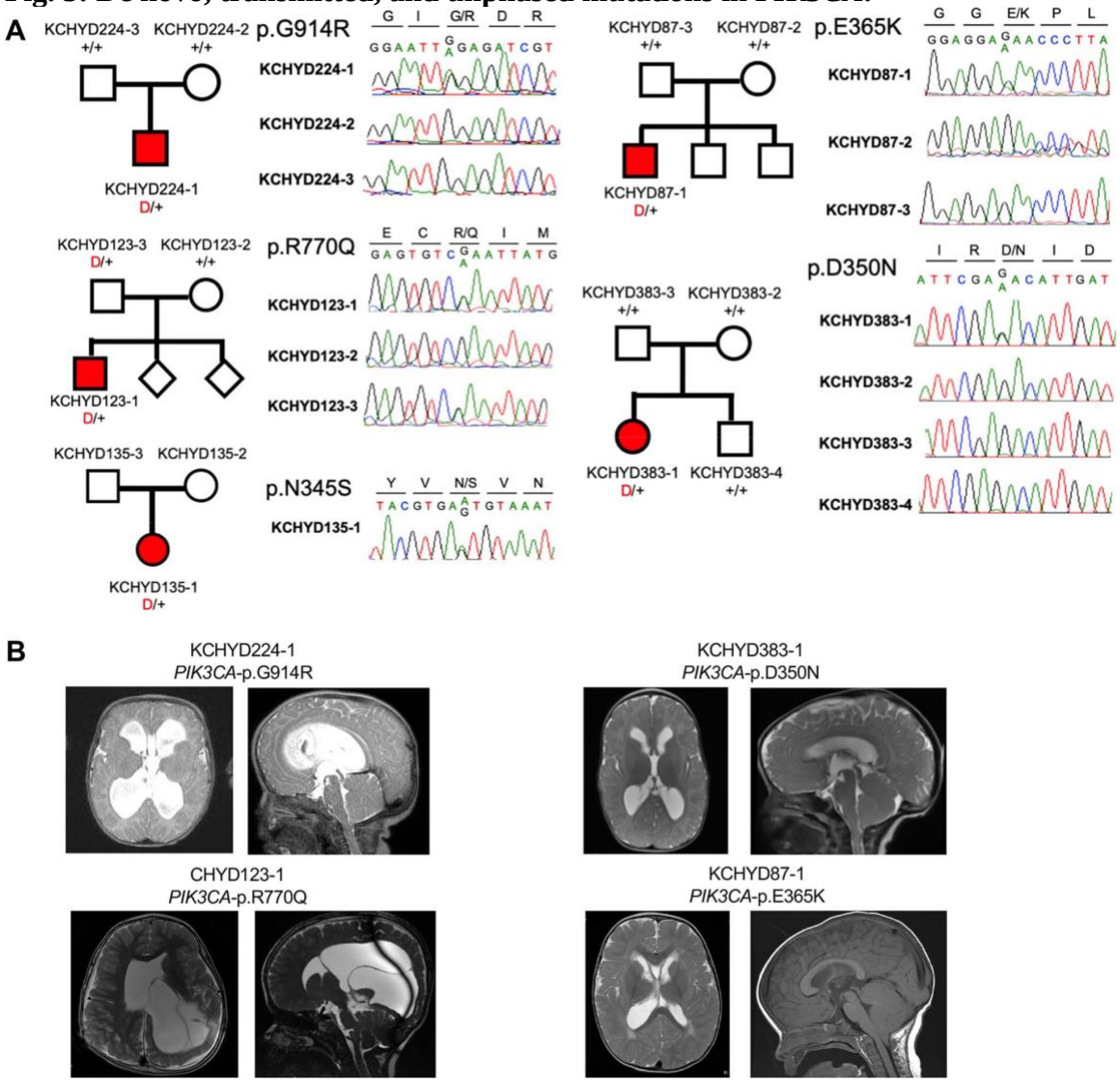

a, Pedigrees and sequencing electropherograms of Sanger sequencing depict all *PIK3CA* mutations in genomic DNA from CH probands. **b,** Representative T1 or T2-weighted brain magnetic resonance images for all available probands.

Fig. 4: De novo, transmitted, and unphased mutations in *PTEN*.

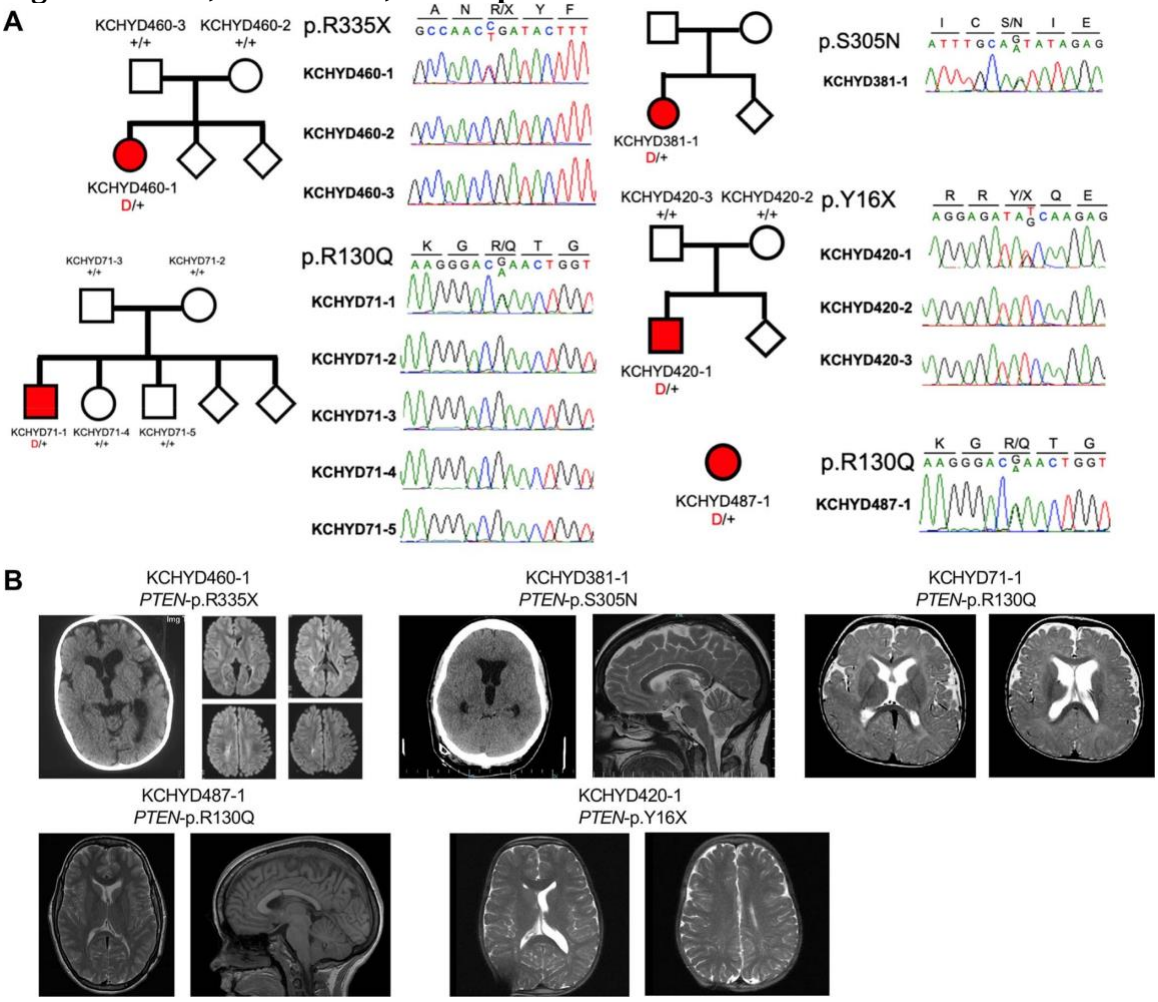

a, Pedigrees and sequencing electropherograms of Sanger sequencing depict all *PTEN* mutations in genomic DNA from CH probands. **b,** Representative T1 or T2-weighted brain magnetic resonance images or head CTs for all available probands.

Fig. 5: De novo, transmitted, and unphased mutations in *MTOR*.

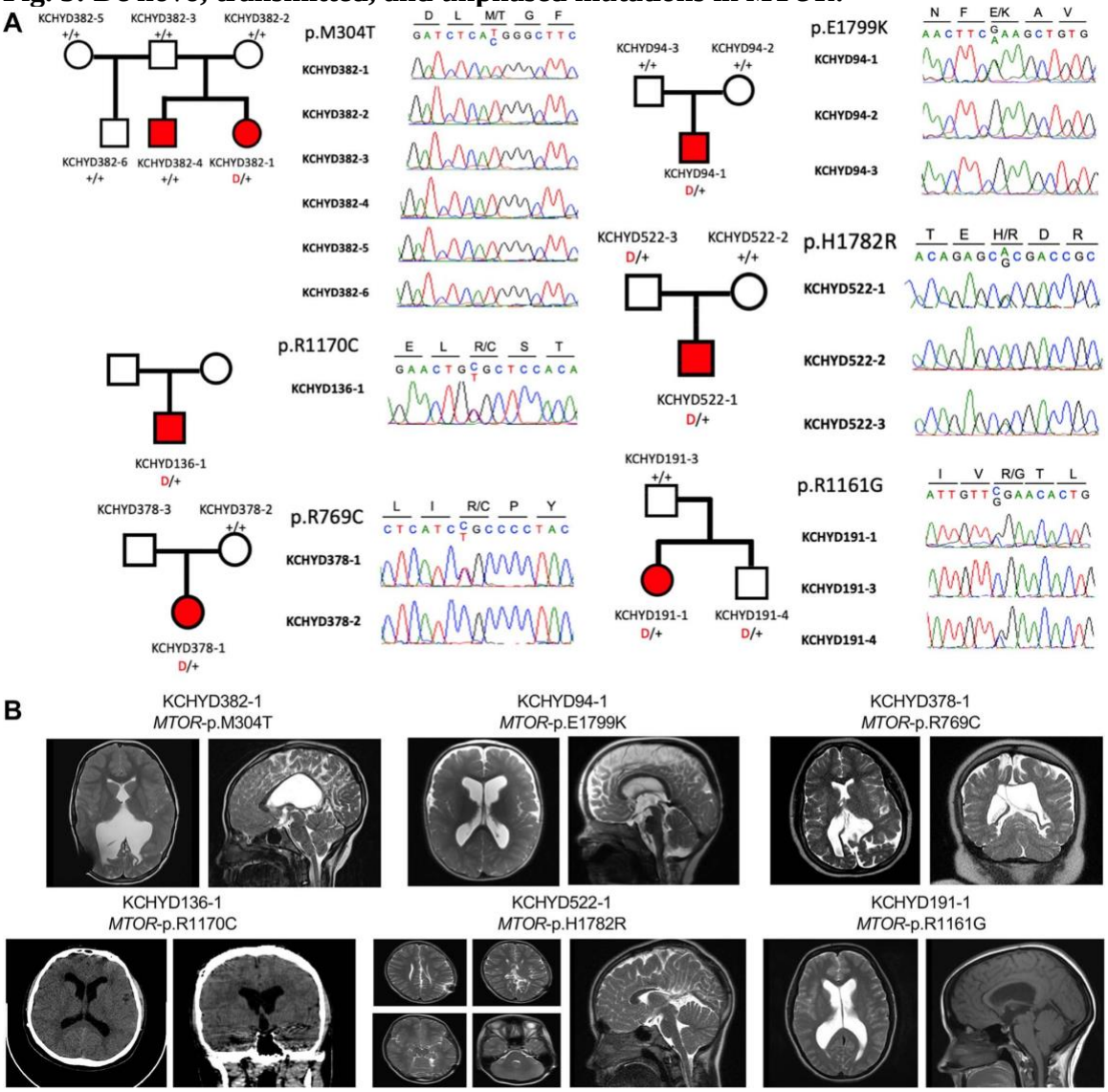

a, Pedigrees and sequencing electropherograms of Sanger sequencing depict all *MTOR* mutations in genomic DNA from CH probands. **b,** Representative T1 or T2-weighted brain magnetic resonance images or head CTs for all available probands.

Fig. 6: De novo and transmitted mutations in *FOXJ1*.

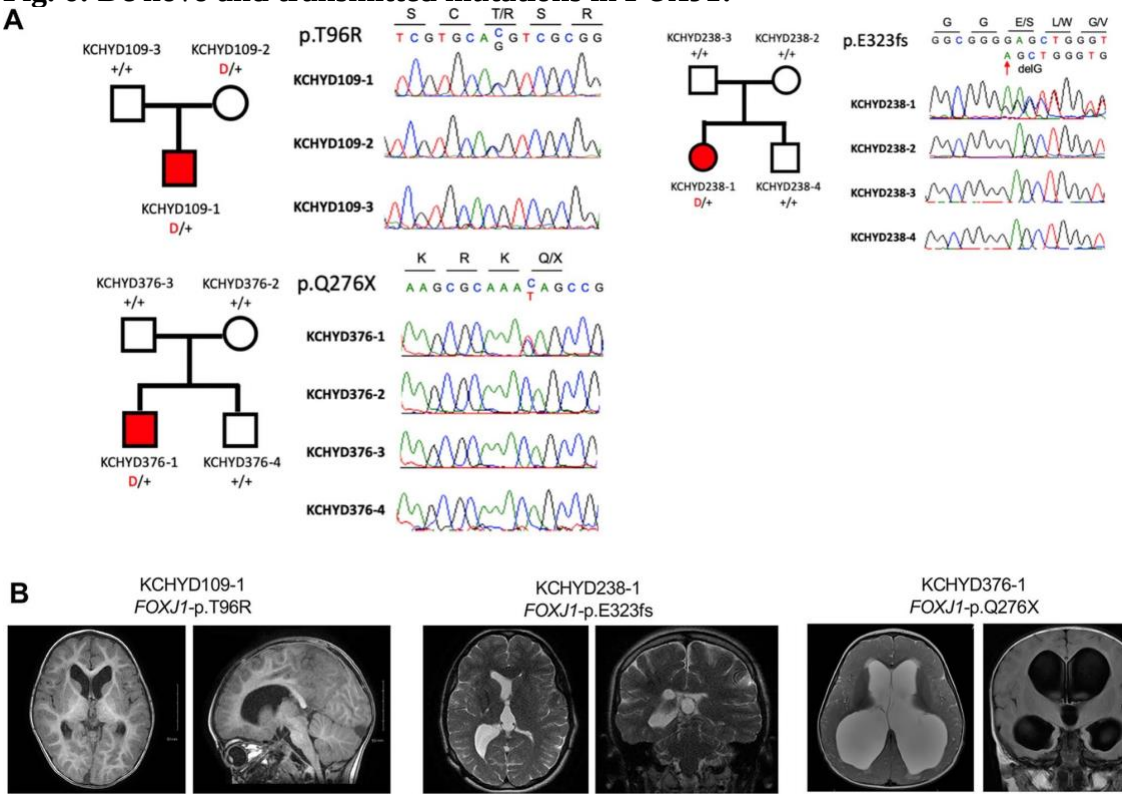

a, Pedigrees and sequencing electropherograms of Sanger sequencing depict all *FOXJ1* mutations in genomic DNA from CH probands. **b,** Representative T1 or T2-weighted brain magnetic resonance images for all available probands.

Fig. 7: De novo and transmitted mutations in *FMN2*.

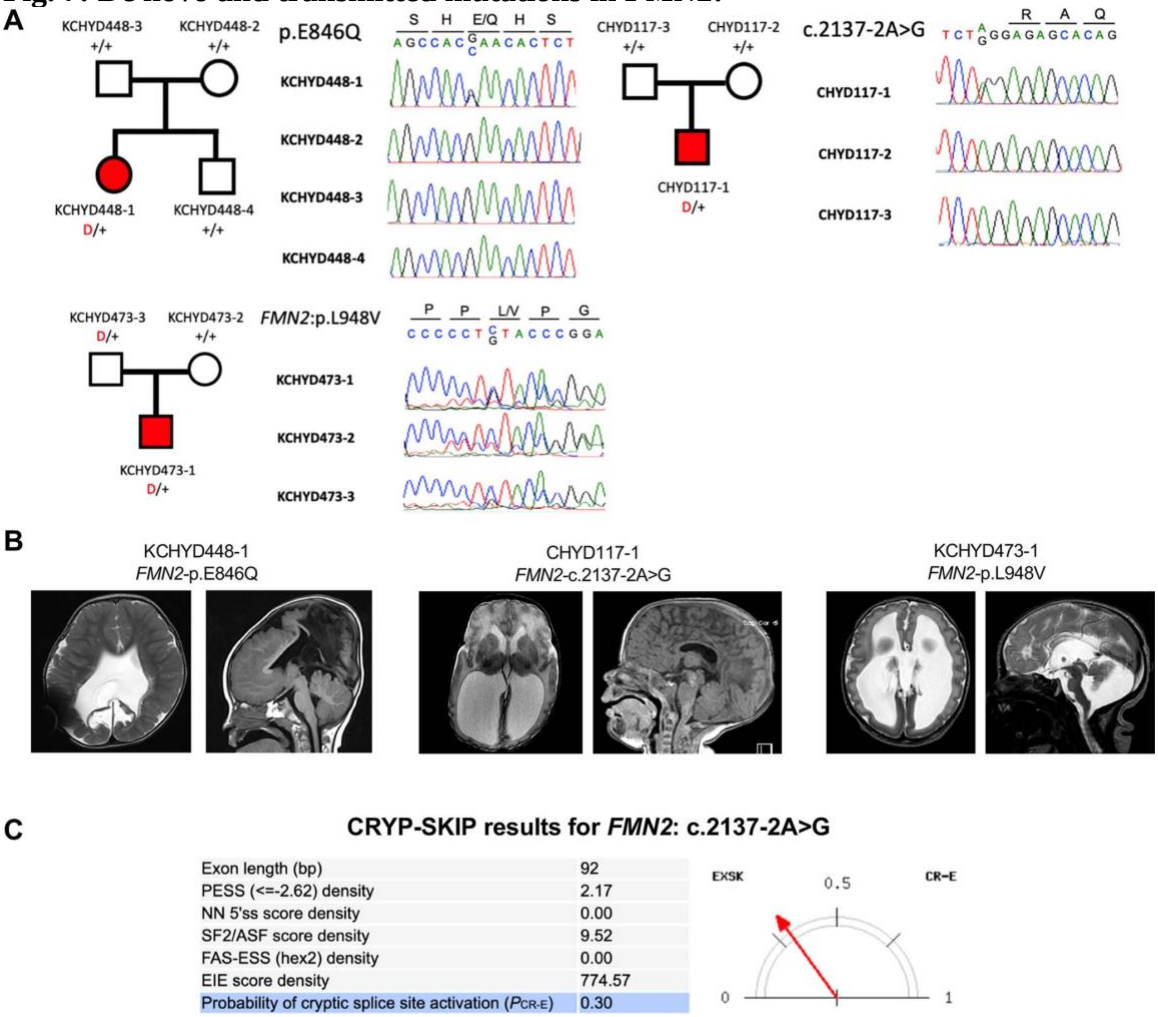

C

CRYP-SKIP results for *FMN2*: c.2137-2A>G

Exon length (bp)	92
PESS (<=-2.62) density	2.17
NN 5'ss score density	0.00
SF2/ASF score density	9.52
FAS-ESS (hex2) density	0.00
EIE score density	774.57
Probability of cryptic splice site activation (P_{CR-E})	0.30

a, Pedigrees and sequencing electropherograms of Sanger sequencing depict all *FMN2* mutations in genomic DNA from CH probands. **b,** Representative T1 or T2-weighted brain magnetic resonance images for all available probands. **c,** The CRYP-SKIP algorithm prediction on splicing defects for FMN2: c.2137-2 A > G.

Fig. 8: De novo, transmitted, and unphased mutations in *PTCH1*.

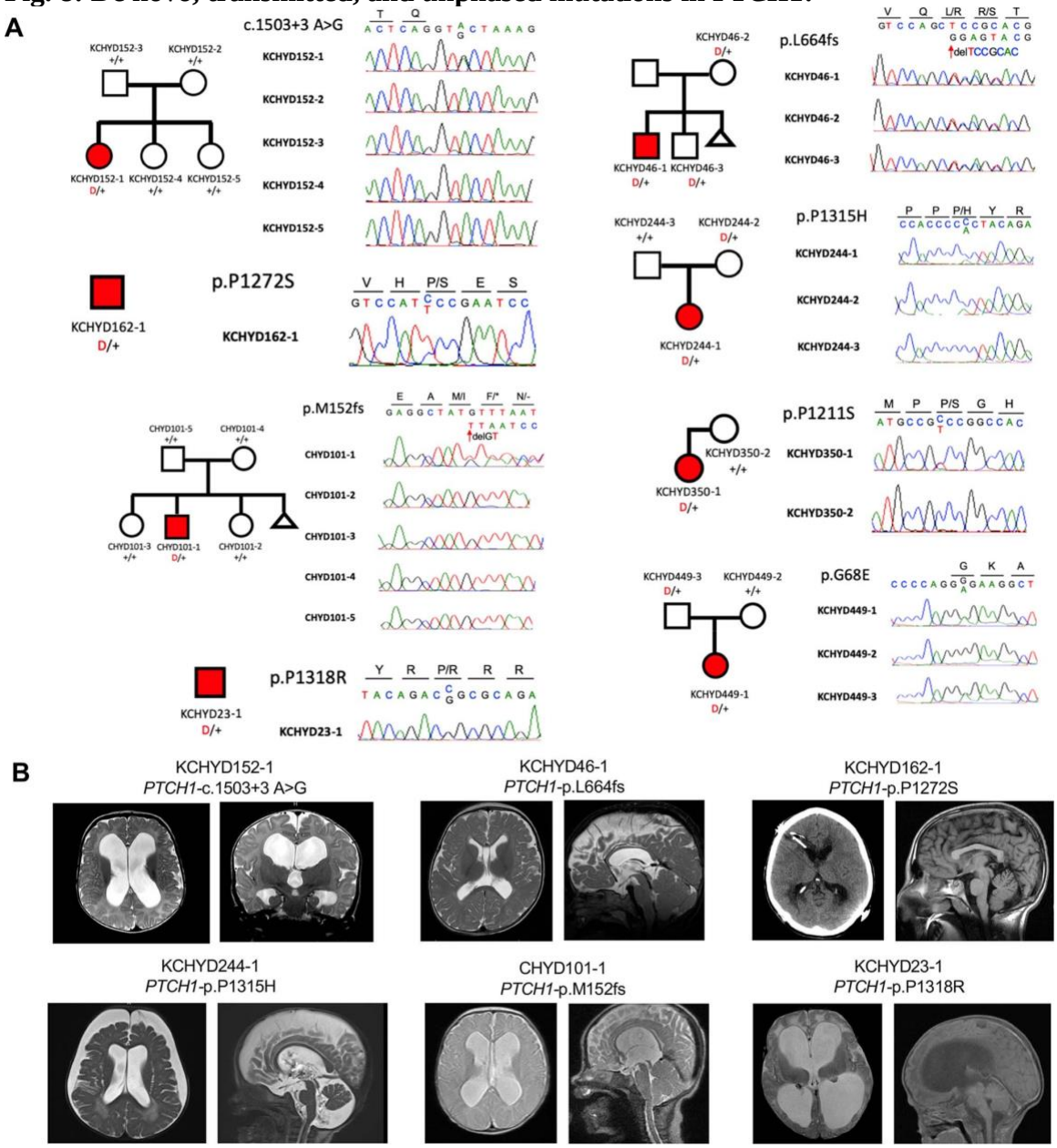

a, Pedigrees and sequencing electropherograms of Sanger sequencing depict all *PTCH1* mutations in genomic DNA from CH probands. **b,** Representative T1 or T2-weighted brain magnetic resonance images or head CTs for all available probands.

Notably, animal and pre-clinical evidence suggests that mutations in these cohort-determined CH risk genes disrupt NSC regulation (**Supplementary Table 11**). *TRIM71*, encoding the RNA-binding protein Tripartite Motif Containing 71, homolog of let-7 (lethal 7) microRNA target lin-41, maintains stem cell pluripotency by the post-transcriptional silencing of target mRNAs via interactions with its RNA-binding NHL domain.[160] *Trim71* deletion in mice results in exencephaly and embryonic lethality by decreasing NSC proliferation.[160] *SMARCC1*, encoding BAF155 subunit of BRG1/BRM-associated factor (BAF; *Saccharomyces cerevisiae* SWI/SNF) chromatin remodeling complex, is an ATP-dependent chromatin remodeler that regulates gene expression required for NSC proliferation, differentiation and survival during telencephalon development.[161] Approximately 80% of mice homozygous for *Smarcc1* missense allele *Baf155*$^{msp/msp}$ exhibit exencephaly similar to *Trim71* mutant mice as a result of defective NSC proliferation and increased apoptosis.[162]

PIK3CA, *PTEN* and *MTOR* are signaling genes of the PI3K pathway. PI3K pathway genes regulate cell growth, proliferation and differentiation in multiple tissues[163], including NSCs in developing ventricular zone[164]. Somatic *PIK3CA* or *MTOR* gain-of-function (GoF) mutations and PTEN LoF mutations drive tumorigenesis by increasing PIP3 levels[165]. Related germline or mosaic mutations have been identified in multiple brain and body overgrowth syndromes that also predispose to cancer.[166] NSC-specific conditional expression of a *Pik3ca* activating allele during mouse embryogenesis induced 100% penetrant, severe nonobstructive murine hydrocephalus with focally increased NSC proliferation and disruption of cell adhesion at the neural-ependymal transition zone.[167] *Pten* conditional deletion in mouse NSCs causes increased PIP3 signaling and severe

obstructive hydrocephalus due to increased ventricular zone NSC proliferation and cell size, with associated cerebral aqueduct obliteration.[168] mTOR inhibitor rapamycin can rescue the severe neonatal hydrocephalus associated with constitutive mTORC1 hyperactivation in NSCs due to primary cilia ablation.[167]

FOXJ1 encodes the forkhead family transcription factor Forkhead Box J1. *Foxj1* depletion in mice causes obstructive hydrocephalus and aqueductal stenosis and disrupts a transcriptional network required for the differentiation of radial glial NSC into multiciliated ependymal cells.[169] *Fmn2* overexpression disrupts neuroepithelial integrity and impairs NSC proliferation and neuronal migration in mouse embryos.[170] *Fmn2* and *FlnA* double knockout mice show significantly thinned cortices and microcephaly associated with NSC proliferation.[171] *Ptch1*$^{+/-}$ mice develop hydrocephalus with incomplete penetrance and variable expressivity.[172] Primary cilia sense gradients of Sonic Hedgehog via PTCH1, which transduces these signals to regulate growth and differentiation of hindbrain NSCs.[173,174]

***FXYD2* contains a significant burden of inherited dominant mutations, including a recurrent splice-site mutation**

To identify additional haplo-insufficient genes associated with CH otherwise not revealed by DNM analysis, we compared the observed and expected number of rare (minor allele frequency (MAF) $\leq 5.0 \times 10^{-5}$) heterozygous LoF mutations in each gene using a one-tailed binomial test while adjusting for gene mutability (**Methods**). *FXYD2* (pLI = 0.24), encoding the regulatory γ-subunit of the Na+/K+-ATPase, surpassed genome-wide significance thresholds (123.5-fold enrichment, $P = 2.3 \times 10^{-6}$; **Fig. 9**). No DNMs or recessive mutations were observed in *FXYD2*. Case–control burden analysis for rare LoF

mutations in all probands versus gnomAD controls also identified *FXYD2* as having high mutational burden in CH probands (odds ratio = 49.3, one-sided Fisher's exact test, $P = 4.8 \times 10^{-5}$). Three unrelated CH probands exhibited two identical transmitted canonical splice-site mutations in *FXYD2* (c.299-1G>A) and one unphased *FXYD2* splice-site mutation (c.410+1G>A) predicted by the CRYP-SKIP algorithm[175] to cause exon skipping (**Fig. 9**). The maximum haplotype shared by the two kindreds (~548 kb) suggests a remote common ancestor (**Supplementary Table 7** and **Supplementary Fig. 2**). Recurrent heterozygous missense mutations in *FXYD2* (p.Gly41Arg) underlie defective Na^+/K^+-ATPase plasma membrane expression and function in autosomal dominant type 2 renal hypomagnesemia (OMIM no. 154020). All *FXYD2* mutant CH probands shared normal serum magnesium levels, and the majority displayed corpus callosum abnormalities and cerebellar tonsillar ectopia (**Supplementary Table 6**).

Fig. 9: Transmitted and unphased mutations in *FXYD2*.

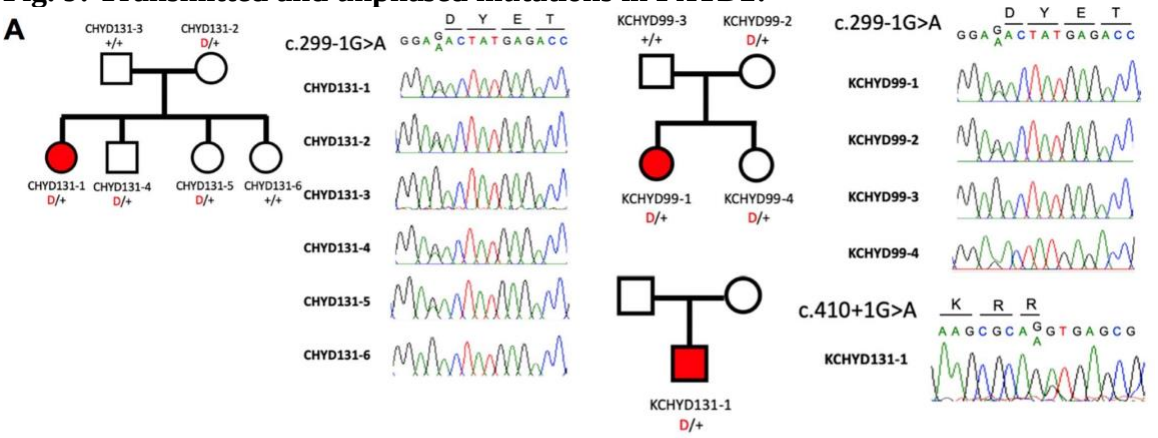

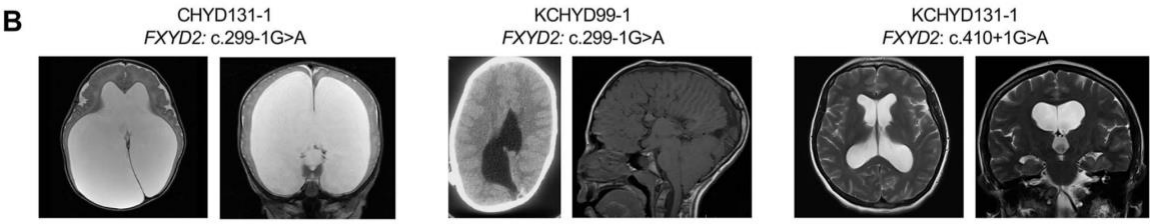

C

CRYP-SKIP results for *FXYD2*: c.299-1G>A

Exon length (bp)	37
PESS (<=-2.62) density	0.00
NN 5'ss score density	0.00
SF2/ASF score density	24.33
FAS-ESS (hex2) density	5.41
EIE score density	505.11
Probability of cryptic splice site activation (P_{CR-E})	0.13

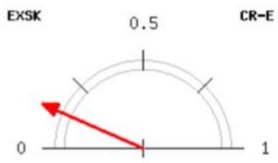

D

CRYP-SKIP results for *FXYD2*: c.410+1G>A

Exon length (bp)	37
PESS (<=-2.62) density	0.00
NN 5'ss score density	0.00
SF2/ASF score density	27.69
FAS-ESS (hex2) density	5.41
EIE score density	535.13
Probability of cryptic splice site activation (P_{CR-E})	0.13

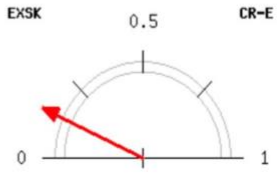

a, Pedigrees and sequencing electropherograms of Sanger sequencing depict all *FXYD2* mutations in genomic DNA from CH probands. **b,** Representative T1 or T2-weighted brain magnetic resonance images for all available probands. **c,** The CRYP-SKIP algorithm prediction on splicing defects for *FXYD2*: c.299-1 G > A. **d,** The CRYP-SKIP algorithm prediction on splicing defects for *FXYD2*: c.410 + 1 G > A.

Recessive genotypes in homologs of mouse hydrocephalus genes are enriched in consanguineous CH cases

The 8.7% consanguinity of our CH cohort (**Supplementary Table 2 and Supplementary Fig. 3**) prompted evaluation for enrichment in CH probands of damaging recessive genotypes (RGs) in homologs of 189 mouse hydrocephalus (mH) genes[7,176] (**Methods**). Among 90 damaging RGs among probands, six occurred in the mH gene set, ($P = 3.7 \times 10^{-3}$) (**Supplementary Table 8a**). Enrichment of RGs in the mH gene set was greater for LoF mutations ($P = 4.9 \times 10^{-4}$; **Supplementary Table 9**). Homozygous RGs new for CH included one each in *POMGNT1* (c.1111-1G>A), *FKRP* (D-Mis p.Gly354Glu), *RHPN1* (p.Met281fs), *CEP290* (c.6012-2A>G), *KCNG4* (p.Gly442Arg) and *KIF19* (p.Gly859fs) (**Supplementary Table 8b** and **Fig. 10**). All probands were products of consanguineous union except the *RHPN1* proband, $P = 1.9 \times 10^{-3}$; **Supplementary Table 10**), revealing a substantial contribution of RGs among probands from consanguineous union (15.6%). Homozygous loss of each of these genes causes severe postnatal hydrocephalus.[7,176]

Fig. 10: Damaging recessive genotypes in human dystroglycanopathy genes and homologs of mouse hydrocephalus genes.

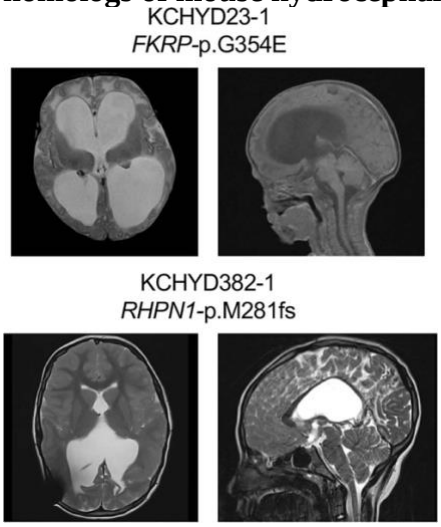

Available clinical-neuroimaging phenotypes of CH probands with damaging recessive mutations.

POMGNT1 and *FKRP* mutations cause human muscular dystrophy-dystroglycanopathy, characterized by hypotonia, seizures, retinal degeneration, cobblestone lissencephaly and, rarely, ventriculomegaly.[177] A set of 12 human muscular dystrophy-dystroglycanopathy genes was enriched among CH probands ($P = 8.5 \times 10{-}5$; **Supplementary Table 8a**) and included *POMGNT2*, a gene with a homozygous (consanguineous) LoF mutation (p.Tyr367X) whose depletion causes hydrocephalus in humans and zebrafish (**Supplementary Table 8b**).[178] Other pathway gene sets implicated in syndromic hydrocephalus[7], including cilia structure and function, cell adhesion, synaptic vesicle biology, planar cell polarity, Ras signaling, Wnt signaling, PI3K-AKT-mTOR signaling and lysosomal storage were not enriched among CH probands (**Supplementary Table 8a**).

CH risk genes converge in fetal human coexpression networks and cell types relevant for fetal neurogenesis

Working from the supposition that CH-associated mutations in biologically pleiotropic genes may disrupt intersecting processes to contribute to a common phenotype[129], we attempted to identify brain specific RNA co-expression networks and cell types in which these genes converge.

Fig. 11: CH risk genes are enriched in a coexpression network pertinent to other neurodevelopmental disorders and in cell types of early fetal neurogenesis.

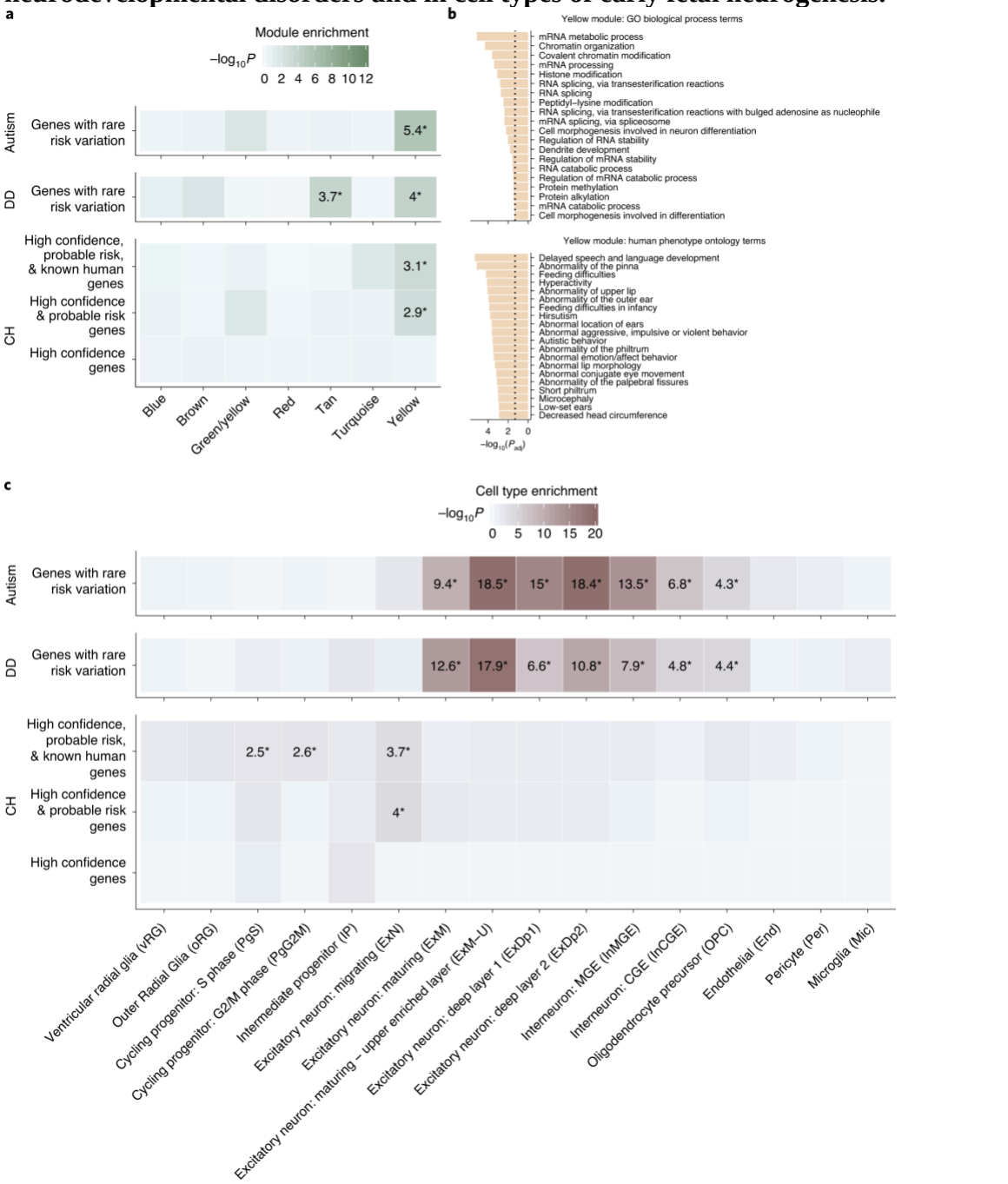

a, Enrichment analysis across weighted gene coexpression network analysis (WGCNA) modules of the midgestational human brain for genes with rare risk variation in CH (high confidence, probable risk and known human genes), ASD and DD (**Methods** contains details of gene set definitions). Only seven modules are shown (labeled by color in line with Walker et al.[155]); other modules demonstrated no significant enrichment for tested gene sets. Tiles labeled with −log10(P value) and an asterisk represent statistically significant enrichment at the Bonferroni multiple-testing cutoff ($\alpha = 0.05/17 = 2.94 \times 10^{-3}$). **b,** Top 20 GO biological process terms and top 20 HP ontology terms enriched for the yellow module. The x axis depicts −log (adjusted P value) and the dotted line represents the $\alpha = 0.05$ significance threshold. (P values are adjusted according to the g:SCS algorithm from g:Profiler[158]). **c,** Enrichment analysis across cell type markers of the midgestational human brain[159] for genes with rare risk variation in CH (high confidence, probable risk and known human genes), ASD and DD. Tiles labeled with −log10(P value) and an asterisk represent significant enrichment at the Bonferroni multiple-testing cutoff ($\alpha = 0.05/16 = 3.13 \times 10^{-3}$).

We tested whether high-confidence, probable and/or known human CH risk genes converge in gene coexpression networks of the midgestational human cortex (**Methods**).[155] Notably, CH risk genes converged in a single transcriptional network ('yellow' module; $P = 1.19 \times 10^{-3}$; **Fig. 11a**), previously associated with ASD and other undiagnosed developmental disorders (DDs).[155] The top enriched Gene Ontology (GO) biological process terms for the yellow module (**Fig. 11b**) include neuronal differentiation and RNA processing (for example, GO: 0000904 and GO: 0048667). The top enriched human phenotype (HP) ontology terms (**Fig. 11b**) describe several congenital defects of craniofacial development and behavioral abnormalities, including 'autistic behavior' (for example, HP: 0000252 and HP: 0000729).

We also examined potential enrichment of CH risk genes in cell type markers of the largest available single-cell (sc)RNA transcriptomic atlas of midgestational brain development44 (spanning 17–18 gestational weeks; **Fig. 11c**). High confidence and probable CH genes were enriched in nascent migrating excitatory neurons ($P = 9.98 \times 10^{-5}$). Adding known human genes to our cohort's risk genes led to additional enrichment in mitotic progenitors PgS ($P = 2.85 \times 10^{-3}$) and PgG2M ($P = 2.44 \times 10^{-3}$). These data suggest that mutations in biologically pleiotropic CH genes disrupt pathways that regulate neurogenesis in the developing human brain.

CH shares genetic risk factors with other neurodevelopmental disorders.

The transcriptional overlap of risk genes for CH, ASD and DD during brain development (**Fig. 4a**); the frequent presence of other neurodevelopmental phenotypes in patients with CH;[179] and the association of ventriculomegaly with ASD[180] and other neuro-developmental conditions[181] prompted our hypothesis that sporadic CH may share common

genetic risk factors with ASD and other neurodevelopmental conditions. Indeed, CH and ASD exhibited significant overlap, with 7 genes harboring LoF DNMs and 20 genes harboring damaging DNMs in both cohorts (**Supplementary Table 12**). CH and other DDs also exhibited significant overlap, with 6 genes harboring LoF DNMs and 22 harboring damaging DNMs in both cohorts (**Supplementary Table 13**). The data suggest partial overlap of genetic risk factors among CH, ASD and other severe neurodevelopmental disorders.

VIII. Discussion

Our WES study of the largest cohort of sporadic, neurosurgically treated CH to date has coupled integrative genomics with deep clinical and neuroradiographic phenotyping to uncover new insights into CH genetic architecture and biology with potential implications for patient care. We show rare mutations with large effect contributed to 22.2% of CH cases (17.7% damaging DNMs, 1.6% RGs, 0.8% transmitted heterozygous LoF variants). Overall, 2.1% of CH cases represented known familial CH mutations. Insertion-deletions, rearrangements, noncoding variants and intronic splice mutations, also likely contribute to genetic risk for CH and will be subjects of future studies. Additional CH cases may arise from complex interactions between genetic and environmental risk factors.

We estimate from the distribution of protein-altering DNMs in LoF-intolerant genes that 34 genes contribute to CH via a DNM mechanism (**Supplementary Fig. 4a; Methods**). This estimate is relatively low compared to the ~400 genes contributing to ASD and CHD, respectively.[150,182] Simulations suggest that sequencing of 2,500 or 5,000 WES trios will yield 90.3% or 97.6% saturation, respectively for CH (**Supplementary Fig. 4b; Methods**). Sequencing of additional trios and isolated probands will therefore detect additional rare mutations with a large effect on disease risk.

These results corroborate and significantly extend our previous work[137], with discovery of new DNMs in *TRIM71* and *SMARCC1* as likely bona fide CH risk genes. We also provide evidence that *PIK3CA*, *PTEN*, *MTOR*, *FOXJ1*, *FMN2*, *PTCH1* and *FXYD2* are new high-confidence sporadic CH genes, collectively accounting for ~7.3% of CH cases. The phenotypes associated with each orthologous gene in corresponding zebrafish

and/or murine disease models support their roles in embryonic neurogenesis and CH pathogenesis (**Supplementary Table 11**).

Several of the identified CH risk genes harboring damaging DNMs and inherited mutations have been implicated in other Mendelian diseases, sometimes producing quite different phenotypes. For example, three CH probands carried mutations in PTEN previously implicated in PTEN hamartoma tumor syndrome (OMIM no. 607174), but none met criteria for this or related PTEN disorders.[183-185] The same is true of a CH proband harboring an MTOR mutation previously implicated in Smith–Kingsmore syndrome (OMIM no. 616638) that did not meet criteria for this disorder.[186] Similarly, although the identical FOXJ1 DNMs in our CH probands were recently identified in patients with type 43 primary ciliary dyskinesia (OMIM no. 618699, associated with bronchiectasis and situs inversus)[187], none of our FOXJ1 mutant patients exhibit these pulmonary or cardiac phenotypes. These observations highlight the phenotypic heterogeneity and variable expressivity associated with these gene mutations, which could arise from environmental modifiers, working in concert with the identified rare mutations and/or specific genetic modifiers, including mosaicism and other somatic mutations.

Much hydrocephalus research has centered on understanding the production, circulation and reabsorption mechanisms of CSF. While these mechanisms are important for acquired hydrocephalus in children and adults or in elderly patients with normal pressure hydrocephalus, our data and much murine data[176] implicate earlier, more fundamental genetic insults in CH. Notably, each high confidence CH gene harboring DNMs is highly expressed in the neuroepithelium lining embryonic neural tube and/or ventricular (VZ) and subventricular (SVZ) zones, where they regulate proliferation,

differentiation and/or fate specification of multipotent NSCs or rapidly proliferative neural precursors. Genetic disruption of embryonic and fetal brain development is therefore the primary event underlying CH pathogenesis in a significant subset of patients.

In this NSC model of CH pathogenesis (**Fig. 5**), nonobstructive ventriculomegaly can result from impaired neurogenesis due to dysregulation in NSC pluripotency, leading to decreased cortical cell mass and a thinned cortical mantle.[188] Obstructive ventriculomegaly can arise from progressive CSF accumulation due to aqueductal obstruction from maldevelopment[189] or to peri-aqueductal NSC hyperproliferation[190]. Other potential mechanisms include impaired growth or size regulation of the ventricular apical domain of primary cilia-containing radial glia NSCs[191] or impaired differentiation of radial glia NSCs into multiciliated ependymal cells.[169] These primary genetic events impairing neuro-gliogenesis could then secondarily disrupt CSF homeostasis by altering normal multiciliated ependymal or possibly glia-lymphatic structure and function. Notably, germinal matrix hemorrhage in premature neonates, the most common cause of acquired pediatric hydrocephalus, is associated with impaired neurogenesis due to ependymal denudation and NSC damage in the VZ-SVZ.[192] An NSC model could thus provide a ‘unified’ mechanism explaining multiple forms of neonatal hydrocephalus, both congenital and acquired.

Fig. 5: A neural stem cell model of sporadic CH.

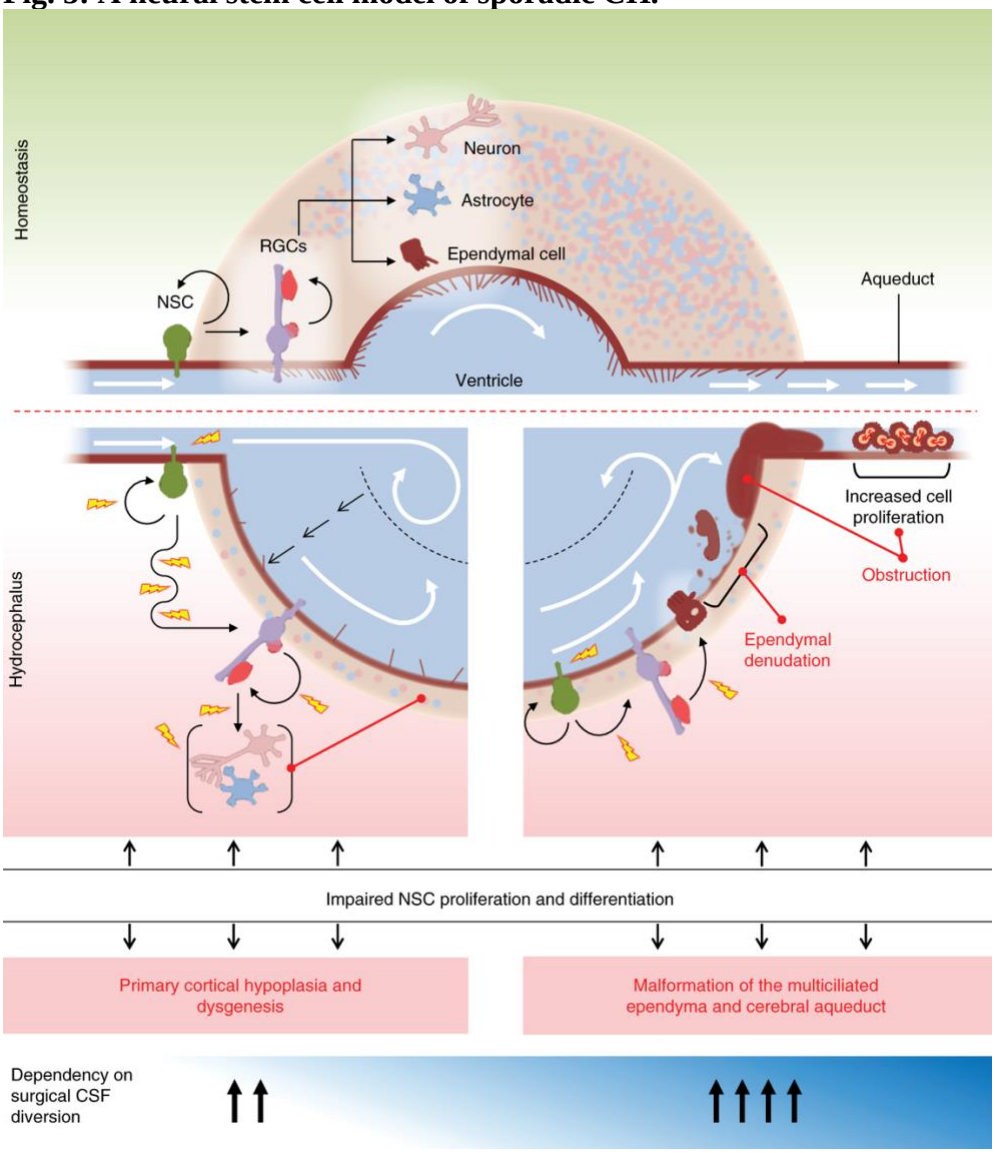

Schematic of the normal developing brain with the ventricular system surrounded by parenchyma consisting of neurons, astrocytes and components of neurogenesis at the cellular level (top). Embryonic and fetal NSC populations, including neuroepithelial cells and radial glia cells (RGCs), together generate virtually all neuronal and glial cells that populate the brain, including multiciliated ependymal cells that line the ventricular system thought to participate in CSF circulation and maintenance of ventricular integrity. Defects in embryonic and fetal NSCs secondary to genetic mutations can thus drive CH via multiple pathogenic mechanisms that impact development and maturation of different cell types. Schematic of two possible developmental mechanisms of NSC alteration that may lead to ventriculomegaly (bottom). In one hypothesized scenario (left), ventriculomegaly results from impaired neurogenesis and an associated decrease in cortical cell mass that reflects a reduction in NSC proliferation. Continued CSF production from the unaffected choroid plexus would further expand the already enlarged ventricular compartment and even at low hydrostatic pressure push the thin, low-resistance cortical ribbon to the dural–bone interface. Ventricular enlargement and dysmorphology could then promote further ventricular expansion through secondary disruption of normal linear CSF laminar flow, eliciting fluid turbulence and current reversal. In another hypothesized scenario (right) that is not necessarily mutually exclusive from the former, altered NSC regulation leads to malformation of ependymal cells and their motile cilia, leading to impaired intraventricular CSF circulation and attendant CSF accumulation responsible for progressive ventricular dilation. Furthermore, defects in cilia-related genes may cause hydrocephalus not only by impairing motile cilia-driven CSF flow, but also by affecting development of primary cilia, which are nonmotile sensory organelles present on embryonic and fetal NSCs, crucial for multiple developmental processes, including patterning, neurogenesis, migration and survival. A combination of defects in NSC patterning and/or the proliferation–differentiation balance can also introduce anatomical defects, resulting in physical obstruction to CSF flow, such as aqueductal stenosis.

Consistent with mutations impacting fundamental aspects of fetal brain development, associated phenotypes such as intellectual disability, neurodevelopmental delay, epilepsy and autistic-like features are not infrequent findings among patients with CH[193], including those of our cohort. In addition, ventricular enlargement in low-birth-weight infants is a risk factor for ASD[194], including those with de novo PTEN mutations. We found enriched overlap of genetic risk factors between CH and ASD and DDs, along with CH risk gene enrichment in coexpression networks previously implicated in these conditions. However, analysis showed convergence of CH risk genes in neural precursors of relatively earlier origin than those of ASD and DDs[195], perhaps accounting for the increased frequency of structural brain abnormalities in CH probands relative to these other disorders. The power of integrative genomics to identify specific cell types and developmental pathways impacted by CH genes will be increased as more high-confidence CH risk genes are discovered.

The diversity of genetic etiologies and underlying biochemical pathways in CH supports implementation of routine clinical WES for newly diagnosed patients. Current recommendations for workup of fetal/neonatal ventriculomegaly include rapid testing for known chromosomal and copy-number abnormalities.[196] However, this strategy does not address CH cases explained by known mutations. Application of routine WES or whole genome sequencing would provide improved diagnosis and management of children with CH. WES or whole genome sequencing could also aid prognostication, increase vigilance for medical screening of mutation-associated conditions (such as cancer surveillance for patients with CH with *PIK3CA* or *PTEN*) and provide recurrence rates to restore reproductive confidence.

In the longer term, we speculate that WES of patients with CH, coupled with deep clinical and neuroradiographical phenotyping, might improve precision of classification schemes to prognosticate neurocognitive outcomes and stratify patients to specific treatments (such as endoscopy versus CSF shunting versus pharmacological therapies). For example, in some nonobstructive CH with excessively thinned cortical mantles from disrupted neurogenesis and normal or even borderline moderately elevated ICPs, surgical CSF shunting may merely expose patients with CH to surgical morbidity without addressing disease pathogenesis. Surgical intervention in these contexts is unlikely to improve associated neurodevelopmental phenotypes such as seizures, motor impairment or intellectual function, more likely arising from genetic disruptions of embryonic neurogenesis than from reversible sequelae of CSF accumulation. These observations should raise thresholds for surgical intervention (or subsequent shunt revision) in patients with CH without obstruction, high ICPs or high-pressure-associated symptoms.

Our data explain ~20% of CH cases; however, most sporadic CH cases remain unexplained. Our current sample size still lacks statistical power adequate to detect the many rare, inherited or sporadic CH-associated risk genes. Although our patients are mostly of European origin, international collaborative studies will soon overcome our current limitations of small cohort size and limited ethnic diversity. Moreover, mechanistic insights into newly identified CH causal genes and core pathways will arise from in vivo experiments in model organisms. Our current work identifying new human gene targets will serve as entry points for these functional studies. Successful pursuit of these next steps will refine current heuristics for clinical decision-making and render personalized treatments for patients with CH, including nonsurgical targeted therapies, a realistic goal.

IX. Supplementary Figures and Tables

Supplementary Figure 1: *De novo* mutation rate closely approximates Poisson distribution in 225 known-CH-gene-negative CH cases and controls. Observed number of *de novo* mutations per subject (bars) compared to the numbers expected (line) from the Poisson distribution in the case (red) and control (blue) cohorts. 'p' denotes two-tailed chi-squared p-value.

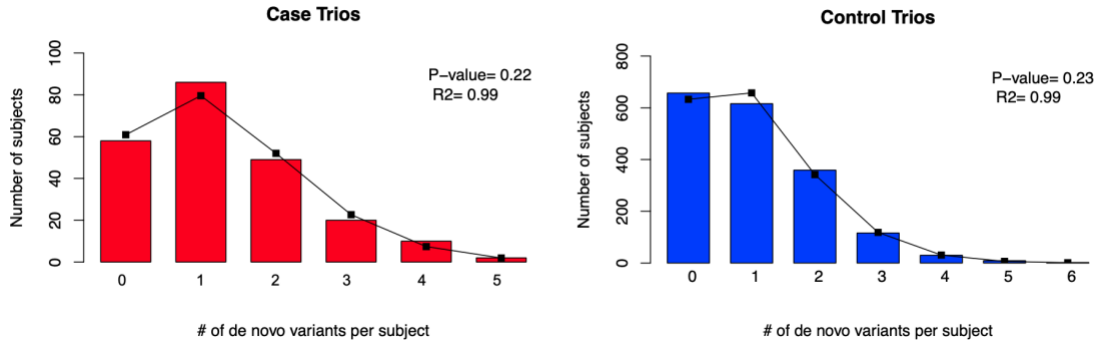

Supplementary Figure 2. Estimation of the mutation age for *FXYD2* . Mutation age (the number of generations, x-axis) was estimated using DMLE+2.3 software based on a Bayesian inference approach. A total of 1,000,000 iterations were performed. The y-axis shows the relative frequency of occurrences for each mutation age estimate. The optimum population growth rate (PGR) and the proportion of sampled chromosome (PSC) for FXYD2c.299-1G>A mutation in the Western European ancestry were estimated to be 0.17 and 0.0000476, respectively. The average mutation age is 52.4 and the 95% confidence interval is between 35.7 and 68.6.

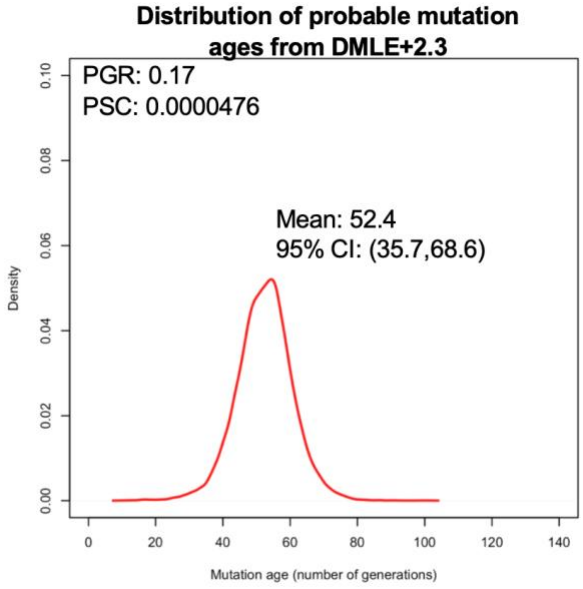

Supplementary Figure 3. Significant difference in the degree of consanguinity between cases and controls. Red and blue dots represent the longest homozygosity-by-descent (HBD) segments and inbreeding coefficients of case **(A)** or control **(B)** subjects, respectively. For reference, the ticks of the x-axis correspond to the inbreeding coefficient for third, second, first cousin, and half-siblings (from smallest to largest). The distribution of the mean inbreeding coefficient **(C)** and longest HBD segment **(D)** respectively between cases and controls was compared using a two-sided Kolmogrov-Smirov non-parametric test.

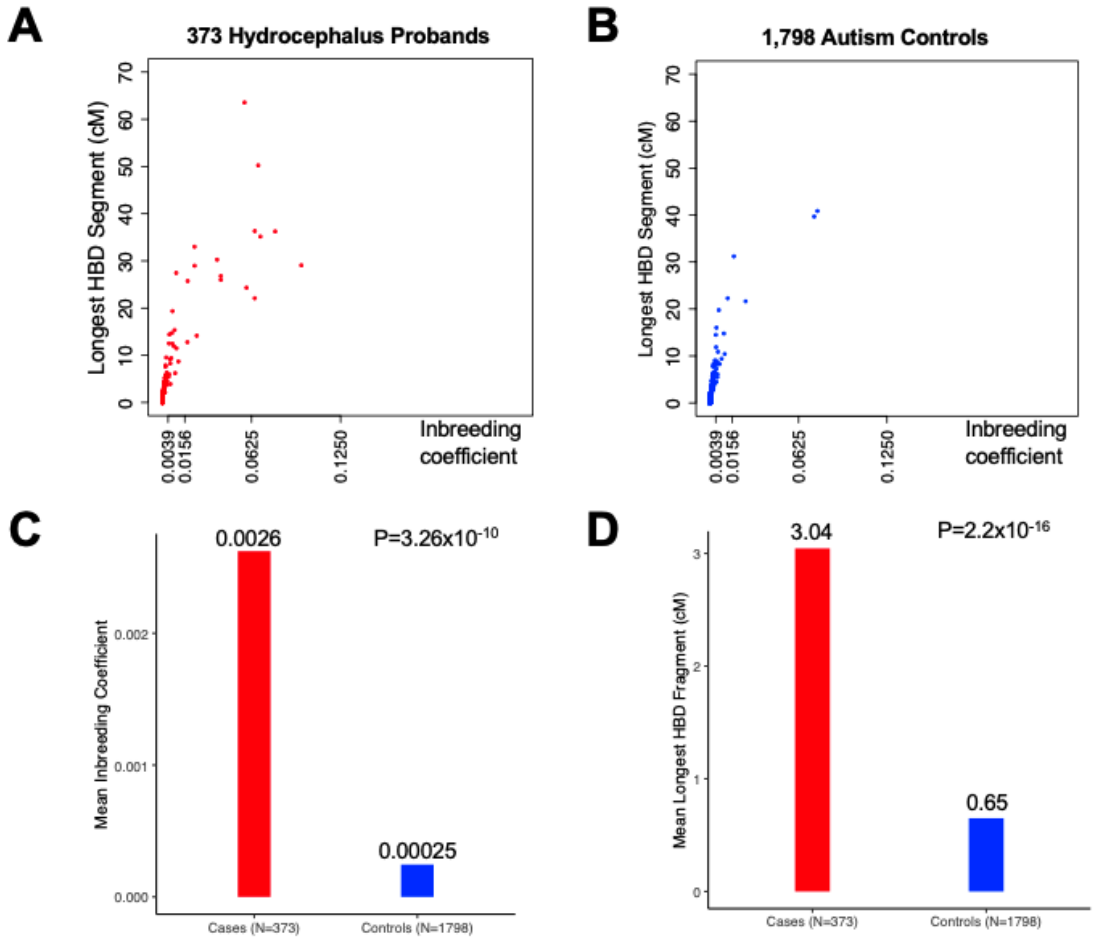

Supplementary Figure 4. CH gene discovery projections. (A) Estimation of the number of CH risk genes via *de novo* mechanism. Monte Carlo simulation was performed based on observed protein-altering *de novo* mutations in 3,049 loss-of-function intolerant genes (pLI ≥ 0.9 in gnomAD [v2.1.1]) using 20,000 iterations. We estimate that the number of risk genes via *de novo* events to be ~34. **(B)** Estimation of the number of recurrent genes. The number of trios and the number of genes with more than one protein- altering *de novo* mutation are specified on the x and y-axis, respectively. We modeled the expected rate of protein altering *de novo* mutations given an increasing sample size. 10,000 iterations were performed to estimate the number of genes with more than 1 protein-altering *de novo* mutations, taking into account the probability of *de novo* protein-altering mutation. WES of 2,500 and 5,000 trios are expected to yield a 90.3% and 97.6% saturation rate, respectively, for all CH risk genes.

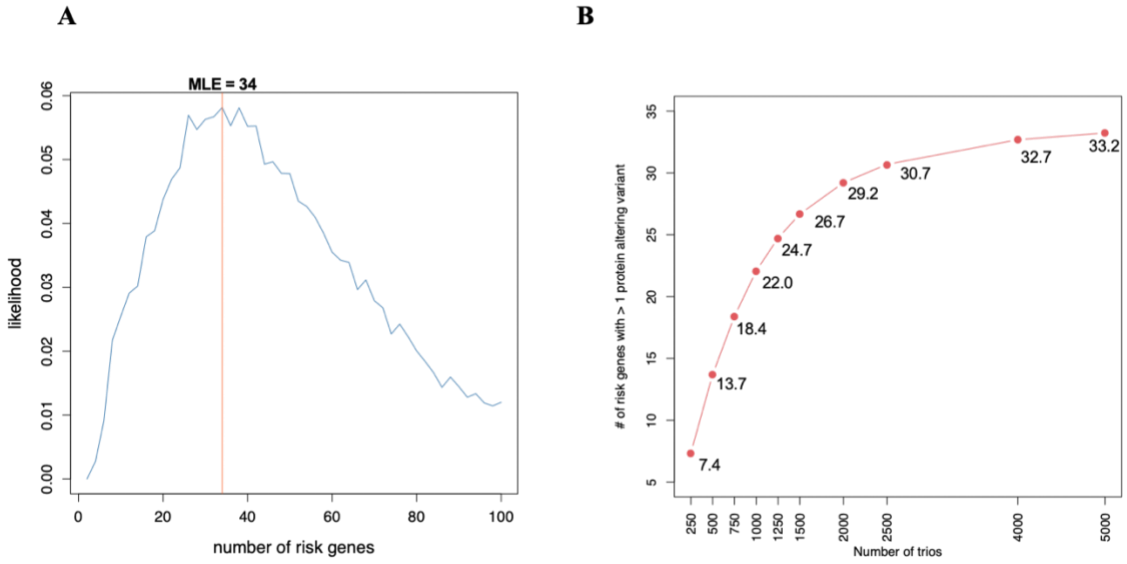

Supplementary Table 1. Number of studied cases and controls

Category	N
# of case trios	232
# of case singletons	149
# of control trios	1,798

N: Number of case trios and singletons, and control trios.

Supplementary Table 2. Demographic characteristics of CH cases and controls

	CH Cases	Autism Sibling Controls
Sample size	381	1,798
Gender		
Male	183 (48.0%)	842 (46.8%)
Female	198 (52.0%)	956 (53.2%)
Ethnicity		
European	304 (79.8%)	1,418 (78.9%)
African American/African*	34 (8.9%)	77 (4.3%)
East Asian	0 (0.0%)	40 (2.2%)
South Asian	7 (1.8%)	88 (4.9%)
Mexican	24 (6.3%)	129 (7.2%)
Other	12 (3.2%)	46 (2.6%)
Truly Consanguineous		
Yes	33 (8.7%)	23 (1.3%)
No	348 (91.3%)	1,775 (98.7%)
Type of Congenital Hydrocephalus		
Non-communicating	211 (55.4%)	N/A
Communicating	123 (32.3%)	N/A
Unknown/Indeterminate	47 (12.3%)	N/A
Known CH Gene Mutation Status		
Positive	8 (2.1%)	N/A
Negative	373 (97.9%)	N/A

* 26 out of 34 classified African Americans/Africans were recruited via the CURE Children's Hospital of Uganda. Of note, recent studies have suggested modern Ugandans show distinct genetic substructure from the HapMap African African populations (Gurdasani 2015 [10.1038/nature13997]; Gurdasani 2019 [10.1016/j.cell.2019.10.004]). The number of samples is shown in each category with the corresponding percentage in parentheses. Ethnicity is determined by principal component analysis compared to HapMap samples using EIGENSTRAT. The criteria of consanguinity are defined as homozygosity in segments of 2cM or greater length that collectively comprise at least 0.35% of the genome. Known CH genes include *L1CAM*, *CCDC88C*, *MPDZ*, *AP1S2*, *EML1*, *WDR81*, *FLNA*, and *CRB2*.

Supplementary Table 3. Summary sequencing statistics for the CH case and control cohorts

Category	Cases (MedExome; N=97)	Cases (xGen IDT; N=748)[&]	Controls (Roche V2; N=5,394)
Read length (bp)	101-148	101	50-99
# of reads per sample (M)	53.1	56.4	111.5
Median coverage at each targeted base (X)	39.2	59.1	68
Mean coverage at each targeted base (X)	45.8	63.2	80.8
% of all reads that map to target	48.80%	57.70%	46.50%
% of all bases that map to target	39.20%	43.40%	35.70%
% of targeted bases read at least 8x	96.50%	98.40%	92.70%
% of targeted bases read at least 10x	95.30%	98.10%	91.40%
% of targeted bases read at least 15x	90.50%	96.60%	87.80%
% Mean error rate	0.30%	0.30%	0.50%

[&]97 case samples were sequenced using the MedExome capture reagent. All other samples were sequenced using the xGEN Exome Research Panel v1.0 capture reagent (IDT). 8X, 10X and 15X were comparable across the platforms.

tics of eight patients with mutations in known familial CH genes. (A) Detailed information about mutations in known familial CH genes. (B) Summary of clinical features of patients with mutations in known familial CH genes.

hnicity	Proband GT	Father GT	Mother GT	Position (GRCh37)	Gene	OMIM Inheritance Model	OMIM Phenotype	Patient Clinical Feature	cDNA Change	AA Change	MetaSVM	MPC	gnomAD WES Freq	gnomAD WGS Freq	BRAVO Freq
ıropean	0/1	0/0	0/1	X:153133291:A:G	*L1CAM*	XLR		Hypotonia, developmental delay, epilepsy, cerebral palsy, cortical visual impairment, obstructive sleep apnea, camptodactyly	c.T1903C	p.W635R	D	1.99	0	0	0
n American	0/1	N/A	N/A	X:153134015:C:A	*L1CAM*	XLR	Hydrocephalus due to aqueductal stenosis (OMIM #: 307000)	N/A	c.1546+1G>T	Splice site	N/A	N/A	0	0	0
ıropean	0/1	0/0	0/1	X:153135592:C:A	*L1CAM*	XLR		Hypotonia, developmental delay, esotropia, camptodactyly, macrocephaly	c.G910T	p.E304X	N/A	N/A	0	0	0
ıropean	0/1	0/0	0/1	X:153135842:C:G	*L1CAM*	XLR		Epilepsy, developmental delay, skeletal abnormalities, macrocephaly	c.806+1G>C	Splice site	N/A	N/A	0	0	0
ıropean	0/1	0/0	0/1	9:13162765:T:TC	*MPDZ*	AR	Non-syndromic Hydrocephalus type 2 (OMIM #: 615219)	Macrocephaly	c.3283dupG	p.E1095fs	N/A	N/A	0	0	0
ıropean	0/1	0/1	0/0	9:13222351:G:A	*MPDZ*	AR			c.C628T	p.Q210X	N/A	N/A	0	0	$8.0x10^{-6}$
ıropean	0/1	0/0	0/1	X:153593833:C:T	*FLNA*	XLD	Periventricular heterotopia	N/A	c.G1451A	p.R484Q	D	1.46	$8.1x10^{-5}$	$6.3x10^{-5}$	$6.4x10^{-5}$
ıropean	0/1	0/0	0/1	X:153578465:G:A	*FLNA*	XLD			c.C7267T	p.P2423S	D	0.53	$4.0x10^{-4}$	$6.0x10^{-4}$	$4.1x10^{-4}$
ıropean	0/1	0/1	0/0	9:126132393:CA:C	*CRB2*	AR	Ventriculomegaly with cystic kidney disease	Exotropia, macrocephaly, developmental delay, epilepsy	c.1062delA	p.T354fs	.	.	0	0	0
ıropean	0/1	0/0	0/1	9:126133821:C:G	*CRB2*	AR			c.C2400G	p.N800K	T	0.55	$2.0x10^{-4}$	0	$9.6x10^{-5}$

ueductal enosis	Corpus callosum abnormalities	White matter volume loss	Developmental delay	Skeletal abnormalities	Macrocephaly	Hypotonia	Ophthal abnormalities	Septal agenesis	Epilepsy	Cerebellar tonsillar ectopia
+	+	+	+	+	-	+	+	+	+	+
+	N/A	N/A	N/A	N/A	N/A	N/A	N/A	N/A	N/A	N/A
+	+	+	+	+	+	+	+	-	-	-
+	+	+	+	+	+	-	-	+	+	-
+	+	+	-	-	+	-	-	+	-	-
N/A	N/A	N/A	N/A	N/A	N/A	N/A	N/A	N/A	N/A	N/A
+	N/A	N/A	-	-	-	-	-	N/A	-	N/A
+	+	+	+	-	+	-	+	+	+	+

; No brain Imaging available for KCHYD268-1, KCHYD133-1, CHYD122-1, . N/A: Not available.

Supplementary Table 5. ***De novo*** **variant enrichment analysis for each mutational class in 225 known-CH-gene negative CH case and control cohorts.**

	Known-CH-gene-negative **Cases, N=225**						**Controls, N=1,798**					
	Observed		**Expected**		**Enrichment**	***p***	**Observed**		**Expected**		**Enrichment**	***p***
	N	**Rate**	**N**	**Rate**			**N**	**Rate**	**N**	**Rate**		
All genes (n=19,347)							**All genes (n=19,347)**					
Total	294	1.31	249.3	1.11	1.18	$3.1x10^{-3}$	Total	1839	1.02	1977.1	1.1	0.93	1
Syn	60	0.27	70.6	0.31	0.85	0.91	Syn	492	0.27	559.8	0.31	0.88	1
T-Mis	139	0.62	123.6	0.55	1.12	0.09	T-Mis	949	0.53	979.3	0.54	0.97	0.84
D-Mis	55	0.24	33.4	0.15	1.65	$3.8x10^{-4}$	D-Mis	248	0.14	266.7	0.15	0.93	0.88
LoF	40	0.18	21.7	0.1	1.85	$2.6x10^{-4}$	LoF	150	0.08	171.3	0.1	0.88	0.95
Protein-altering	234	1.04	178.7	0.79	1.31	$4.3x10^{-5}$	Protein-altering	1347	0.75	1417.3	0.79	0.95	0.97
Protein-damaging	95	0.42	55.1	0.24	1.72	$6.6x10^{-7}$	Protein-damaging	398	0.22	438	0.24	0.91	0.98
High brain-expressed genes (brain expression rank ≥ 75%; n=4,522)							**High brain-expressed genes (brain expression rank ≥ 75%; n=4,522)**					
Total	94	0.42	64.3	0.29	1.46	$3.0x10^{-4}$	Total	515	0.29	511.6	0.28	1.01	0.45
Syn	15	0.07	18	0.08	0.84	0.79	Syn	128	0.07	143	0.08	0.9	0.9
T-Mis	39	0.17	30.6	0.14	1.27	0.08	T-Mis	274	0.15	243.6	0.14	1.12	0.03
D-Mis	23	0.1	9.9	0.04	2.33	$2.5x10^{-4}$	D-Mis	74	0.04	78.9	0.04	0.94	0.72
LoF	17	0.08	5.8	0.03	2.92	$1.2x10^{-4}$	LoF	39	0.02	46.2	0.03	0.85	0.87
Protein-altering	79	0.35	46.3	0.21	1.71	$7.8x10^{-6}$	Protein-altering	387	0.22	368.6	0.21	1.05	0.18
Protein-damaging	40	0.18	15.7	0.07	2.55	$2.0x10^{-7}$	Protein-damaging	113	0.06	125	0.07	0.9	0.87
Loss-of-function intolerant genes (gnomADv2.1.1 pLI ≥ 0.9; n=3,049)							**Loss-of-function intolerant genes (gnomADv2.1.1 pLI ≥ 0.9; n=3,049)**					
Total	87	0.39	59.8	0.27	1.45	$5.7x10^{-4}$	Total	456	0.25	473.5	0.26	0.96	0.83
Syn	14	0.06	16.8	0.07	0.83	0.79	Syn	115	0.06	133.4	0.07	0.86	0.96
T-Mis	30	0.13	27	0.12	1.11	0.31	Mis	233	0.13	213.5	0.12	1.08	0.12
D-Mis	25	0.11	10.6	0.05	2.35	$1.2x10^{-4}$	D-Mis	75	0.04	84.5	0.05	0.88	0.87
LoF	18	0.08	5.3	0.02	3.37	$1.3x10^{-5}$	LoF	33	0.02	42.2	0.02	0.78	0.94
Protein-altering	73	0.32	43	0.19	1.7	$1.9x10^{-5}$	Protein-altering	341	0.19	340.2	0.19	1	0.53
Protein-damaging	43	0.19	16	0.07	2.69	$1.6x10^{-8}$	Protein-damaging	108	0.06	126.7	0.07	0.85	0.96
Loss-of-function-intolerant & high brain expressed genes (n=1,495)							**Loss-of-function-intolerant & high brain expressed genes (n=1,495)**					
Total	53	0.24	28.6	0.13	1.85	$2.8x10^{-5}$	Total	228	0.13	227.9	0.13	1	0.51
Syn	8	0.04	7.9	0.04	1.01	0.54	Syn	58	0.03	63.3	0.04	0.92	0.76
T-Mis	16	0.07	12.8	0.06	1.25	0.22	Mis	112	0.06	102.2	0.06	1.1	0.18
D-Mis	16	0.07	5.2	0.02	3.08	$1.1x10^{-4}$	D-Mis	41	0.02	41.5	0.02	0.99	0.55
LoF	13	0.06	2.6	0.01	4.94	$4.2x10^{-6}$	LoF	17	0.01	20.9	0.01	0.81	0.83
Protein-altering	45	0.2	20.7	0.09	2.18	$2.4x10^{-6}$	Protein-altering	170	0.1	164.6	0.09	1.03	0.35
Protein-damaging	29	0.13	7.8	0.03	3.71	$5.0x10^{-9}$	Protein-damaging	58	0.03	62.4	0.03	0.93	0.73

N: number of *de novo* mutations; Rate: number of *de novo* mutations per subject; Enrichment: ratio of observed to expected numbers of *de novo* mutations; D-Mis: damaging missense mutations as predicted by MetaSVM or MPC-2; LoF: loss-of-function mutations comprised of premature termination, frameshift or splice site mutation; High brain-expressed genes denote genes in the top quartile of expression in the developing mouse brain; Loss-of-function-intolerant genes denote genes with a pLI ≥ 0.9 in the gnomAD database (v2.1.1).

Supplementary Table 6. Summary of clinical features of patients with (A) *FOXJ1*, *FMN2*, (B) *PTCH1,* or (C) *FXYD2* mutations

A

Subjects	Treatment	Aqueductal stenosis	Corpus callosum abnormalities	Septal agenesis	Developmental delay	Megalencephaly	Colpocephaly	Interhemispheric cyst	Craniofacial abnormalities	Cardiac abnormalities	Hearing loss	Dysraphism/ Neural tube defect	Macrocephaly	Other cerebellar abnormalities	Epilepsy	Cavum septum pellucidum
KCHYD238-1	ETV > Shunted	+	-	-	+	-	-	-	-	-	-	-	-	-	-	-
KCHYD376-1	ETV > Shunted	+	-	-	+	-	-	-	-	-	-	-	-	-	-	+
KCHYD109-1	Shunted	+	-	-	+	-	-	-	-	-	-	-	-	-	-	+
KCHYD448-1	Shunted	+	+	+	-	+	+	+	+	+	+	-	-	-	-	-
CHYD117-1*	Shunted	+	+	+	+	-	-	-	-	-	-	+	+	-	-	-
KCHYD473-1*	Shunted	+	+	-	+	-	-	-	-	-	-	-	-	+	+	+

ETV: Endoscopic third ventriculostomy. *CHYD117-1 and KCHYD473-1 meet diagnostic criteria for Mental retardation syndrome 47

B

Subject[δ]	Treatment	Aqueductal stenosis	Cavum septum pellucidum	Craniofacial abnormalities	Developmental delay	Megalencephaly	Cerebellar tonsillar ectopia	Skeletal abnormalities	Other cerebellar abnormalities	Hearing loss	Corpus callosum abnormalities	Intracranial cyst	Macrocephaly
CHYD101-1	Shunted	+	+	+	+	+	+	+	-	-	-	-	-
KCHYD152-1	Shunted	+	-	+	-	+	+	-	+	-	-	-	-
KCHYD46-1	Shunted	-	+	-	-	-	-	-	-	-	-	-	-
KCHYD244-1	Shunted	-	-	+	-	-	-	-	+	-	-	-	+
KCHYD449-1	Shunted	+	N/A	-	-	N/A	N/A	+	N/A	-	N/A	N/A	-
KCHYD162-1	Shunted	+	+	+	+	+	-	-	-	+	-	-	-
KCHYD23-1	Shunted	+	+	+	-	-	-	-	-	-	+	-	-
NG2288-1	N/A	N/A	N/A	N/A	N/A	N/A	N/A	N/A	N/A	N/A	N/A	N/A	N/A
KCHYD350-1	N/A	-	N/A	-	+	N/A	N/A	-	+	-	+	N/A	+

[δ]KCHYD152-1 and KCHYD46-1 meet criteria for Gorlin syndrome; KCHYD244-1 meets diagnostic criteria for Anterior Segment Dysgenesis Syndrome; No brain Imaging available for KCHYD449-1 and NG2288-1.

C

Subject	Treatment	Aqueductal stenosis	Corpus callosum abnormalities	Cerebellar tonsillar ectopia	Interhemispheric cyst	Septal agenesis	Epilepsy	Intracranial cyst	Polymicrogyria	Developmental delay	Craniofacial abnormalities	Hernia
KCHYD131-1	Shunted	-	-	-	-	-	-	-	-	-	-	-
CHYD131-1	Shunted	+	+	+	+	+	+	-	-	-	-	-
KCHYD99-1	Shunted	-	+	+	-	-	-	+	+	+	+	+

Supplementary Table 7. Haplotypes flanking *FXYD2*$^{c.299\text{-}1G>A}$ in two kindreds support to recent shared ancestry

Chr 11 Pos.	Rs #	Bravo Freq	CHYD131-1 Inferred Haplotype	KCHYD99-1 Inferred Haplotype	CHYD131-1 GT	CHYD131-2 GT	CHYD131-3 GT	KCHYD99-1 GT	KCHYD99-2 GT	KCHYD99-3 GT
117309495	rs10892104	0.395	A	G	A|G	A|G	G|G	G|G	G|G	G|A
117309527	rs75808396	0.143	A	G	A|G	A|G	G|G	G|G	G|G	G|A
117309581	rs61905269	0.11	G	G	G|G	G|G	G|G	G|A	G|G	A|G
117329415	rs520328	0.112	G/A	G	G/A	G/A	G/A	G|G	G|G	G|G
117332343	rs2298766	0.238	C	C	C|C	C|C	C|C	C|T	C|C	T|T
117332352	rs588048	0.995	G	G	G|G	G|G	G|G	G|G	G|G	G|G
117335722	rs538847	0.647	T/C	T	T/C	T/C	T/C	T|C	T|T	C|C
117335991	rs663191	0.059	C	C	C|C	C|C	C|T	C|C	C|C	C|C
117351353	rs577166	0.06	C	C	C|C	C|C	C|T	C|C	C|C	C|C
117375596	rs2276343	0.188	G	G	G|G	G|G	G|A	G|G	G|G	G|G
117375853	rs141701802	0.005	C	C	C|C	C|C	C|C	C|C	C|T	C|C
117389517	rs3819210	0.209	A	A	A|A	A|A	A|G	A|A	A|A	A|A
117391736	rs7936795	0.152	A	A	A|A	A|A	A|G	A|A	A|A	A|A
117391966	rs2276340	0.153	G	G	G|G	G|G	G|A	G|G	G|G	G|G
117392110	rs35503235	0.032	A	A	A|A	A|A	A|A	A|A	A|G	A|A
117395481	rs2276339	0.208	G	G	G|G	G|G	G|A	G|G	G|G	G|G
117403017	rs7109567	0.618	G	G	G|G	G|G	G|A	G|G	G|A	G|G
117403235	rs3741280	0.351	G	G	G|G	G|G	G|T	G|G	G|T	G|G
117647461	rs73587457	0.101	C	C	C|G	C|C	G|C	C|C	C|C	C|C
117667688	rs113876980	0.221	C	C	C|C	C|A	C|A	C|C	C|A	C|A
117691386	rs869789	0.135	G	G	G|A	G|G	A|G	G|G	G|G	G|G
117693196	***c.299-1G>A***	**1.6x10^{-5}**	**T**	**T**	**T|C**	**T|C**	**C|C**	**T|C**	**T|C**	**C|C**
117693255	rs529623	0.458	T	T	T|T	T|C	T|C	T|T	T|C	T|C
117698762	rs7117314	0.317	G	G	G|G	G|G	G|A	G|G	G|A	G|A
117772848	rs491822	0.405	C/T	T	C/T	C/T	C/T	T|C	T|C	C|C
117773110	rs494457	0.959	C	C	C|C	C|C	C|C	C|C	C|C	C|C
117774146	rs2186627	0.27	C	C	C|G	C|C	G|C	C|G	C|G	G|G
117774291	rs2845712	0.878	C	C	C|C	C|C	C|C	C|C	C|C	C|C
117776471	rs3802873	0.253	C	C	C|C	C|C	C|C	C|T	C|T	T|T
117776526	rs3802872	0.457	A/G	G	A/G	A/G	A/G	G|A	G|A	A|A
117779612	rs947969	0.495	G/A	A	G/A	G/A	G/A	A|G	A|G	G|G
117780744	rs12801855	0.115	C/T	C	C/T	C/T	C/T	C|C	C|C	C|C
117781435	rs2155194	0.952	G	G	G|G	G|G	G|G	G|G	G|G	G|G
117782638	rs2277288	0.297	A	A	A|A	A|A	A|A	A|G	A|G	G|G
117784434	rs11605749	0.245	G	G	G|C	G|C	C|C	G|G	G|G	G|G
117784714	rs11216618	0.195	T/C	T	T/C	T/C	T/C	T|T	T|T	T|T
117785260	rs4936410	0.242	C	C	C|T	C|T	T|T	C|C	C|C	C|C
117799923	rs7928668	0.608	T	T/C	T|T	T|T	T|T	T/C	T/C	T/C
117800033	rs35251396	0.043	G	G	G|G	G|G	G|G	G|G	G|A	G|G
117800083	rs10892196	0.607	T	T/C	T|T	T|T	T|T	T/C	T/C	T/C
117857338	rs10892202	0.12	G	G	G|G	G|C	G|G	G|G	G|G	G|C
117858983	rs4252248	0.71	G	A	G|A	G|A	A|A	A|A	A|A	A|A
117859209	rs4252249	0.121	G	G	G|G	G|A	G|G	G|G	G|G	G|A

The inferred haplotype for SNPs flanking *FXYD2*$^{c.299\text{-}1G>A}$ mutation in 2 kindreds (KCHYD99 and KCHYD131) are shown. The maximum haplotype shared by 2 kindreds is ~548kb, indicated by gray. To the right of the columns showing inferred haplotypes, the genotypes (GT) of SNPs at each position in each family member are indicated. Chr 11 Pos., position on chromosome 11 in hg37; rs#, SNP identifier in dbSNP database (the novel mutation shared by 2 kindreds is denoted by *c.299-1G>A*); Bravo Freq: frequency of minor allele in the Bravo database.

Supplementary Table 8. Recessive genotypes (RGs) in homologs of mouse hydrocephalus genes are enriched in CH cases. (A) Results from a one-tailed binomial test for damaging RGs in curated gene sets in CH cases and controls were shown. The expected number of damaging RGs was determined on the basis of fitted values from the polynomial regression model using the damaging de novo probabilities ad described (Jin et al. 2017). Damaging RGs in the human dystroglycanopathy and mouse CH gene sets were enriched in CH probands. RGs were not enriched among CH probands in genes encoding proteins previously implicated in Mendelian syndromes in which hydrocephalus has been reported (Kousi and Katsanis 2016), including PI3K-ATK-mTOR signaling, planar cell polarity, synaptic vesicle cycle, Ras signaling, and lysosomal storage disorder gene sets. The dystroglycanopathies genes were extracted from Kousi et al. (Kousi and Katsanis 2016). Gene sets encoding cell adhesion molecules, Wnt signaling, PI3K-ATK-mTOR pathway, synaptic vesicle cycle, Ras signaling pathway and lysosomal storage disorders were curated based on KEGG, pathway database and HUGO Gene Nomenclature. Planar cell polarity gene lists were curated based on definitive reviews from Wang et al. 2019 and Tissir et al. 2013. The testing results for gene sets without damaging RGs in cases were not shown.The Bonferroni multiple-testing cutoff is $5.0x10^{-3}$ (=0.05/(5x2)). N/A: Not available. **(B)** Characteristics of patients with damaging RGs in the human dystroglycanopathy and mouse CH gene sets.

A

Gene Set (# genes)	Observed				Expected	Enrichment	P-value
	Homozygous	Compound heterozygous	Unique genes	Recessive genotypes	Recessive genotypes		
373 Hydro Cases							
All genes (19,347)	69	21	89	90	-	-	-
Mouse hydrocephalus genes (189)	6	0	6	6	1.47	4.08	**$3.7x10^{-3}$**
Dystroglycanopathies (12)	3	0	3	3	0.08	36.3	**$8.5x10^{-5}$**
Ciliopathies genes (22)	1	0	1	1	0.29	3.45	0.25
Cell adhesion molecules (142)	1	0	1	1	0.69	1.46	0.5
Wnt signaling pathway (156)	1	0	1	1	1.11	0.89	0.68
1,798 Controls							
All genes (19,347)	39	144	164	183	-	-	-
Mouse hydrocephalus genes (189)	1	1	2	2	3.71	0.54	0.89
Dystroglycanopathies (12)	0	0	0	0	0.18	0	1
Ciliopathies genes (22)	0	0	0	0	0.88	0	1
Cell adhesion molecules (142)	0	1	1	1	1.34	0.75	0.74
Wnt signaling pathway (156)	0	1	1	1	2.7	0.37	0.93

B

Proband ID	Ethnicity	Truly consanguineous?	Gene	Position (GRCh37)	Type	OMIM Inheritance Model	cDNA Change	AA Change	MetaSVM	mpc	gnomad WES Freq	gnomad WGS Freq	Bravo Freq	Gene set
NG3001-1	South Asian	Yes	*POMGNT1*	1:46658888:C:T	Hom	AR	c.1111-1G>A	Splice	.	.	$4.1x10^{-6}$	0	$8.0x10^{-6}$	Dystroglycanopathies, Mouse
NG1961-1	European	No	*POMGNT2*	3:43121823:A:T	Hom	AR	c.T1101A	p.Y367X	.	.	0	0	0	Dystroglycanopathies
KCHYD23-1	European	Yes	*FKRP*	19:47259768:G:A	Hom	AR	c.G1061A	p.G354E	D	1.3	$1.0x10^{-4}$	$3.2x10^{-5}$	$4.0x10^{-5}$	Dystroglycanopathies, Mouse
KCHYD382-1	Undetermined	No	*RHPN1*	8:144461573:GAT:G	Hom	N/A	c.841_842del	p.M281fs	.	.	$2.0x10^{-4}$	$2.0x10^{-4}$	$2.4x10^{-4}$	Mouse
NG2276-1	European	Yes	*CEP290*	12:88462424:T:C	Hom	AR	c.6012-2A>G	Splice	.	.	$4.3x10^{-6}$	.	$1.6x10^{-5}$	Mouse
KCHYD282-1	African American	Yes	*KCNG4*	16:84256059:C:T	Hom	N/A	c.G1324A	p.G442R	D	0.3	$2.0x10^{-4}$	$9.0x10^{-4}$	$9.6x10^{-4}$	Mouse
NG1188-1	European	Yes	*KIF19*	17:72350566:CG:C	Hom	N/A	c.2575delG	p.G859fs	.	.	$3.0x10^{-4}$	$9.7x10^{-5}$	$2.0x10^{-4}$	Mouse

Supplementary Table 9. Loss-of-function recessive genotypes in the mouse hydrocephalus and dystroglycanopathies gene sets are more enriched in CH cases compared to damaging recessive genotypes.

Gene Set (# genes)	Observed				Expected	Enrichment	P-value
	Homozygous	Compound heterozygous	Unique genes	Recessive genotypes	Recessive genotypes		
373 Hydro Cases							
All genes (19,347)	28	2	30	30	-	-	-
Mouse hydrocephalus genes (189)	4	0	4	4	0.37	10.79	$4.9x10^{-4}$
Dystroglycanopathies (12)	2	0	2	2	0.02	103.76	$1.8x10^{-4}$
Ciliopathies genes (22)	1	0	1	1	0.06	16.47	0.06
Cell adhesion molecules (142)	1	0	1	1	0.22	4.62	0.2
Wnt signaling pathway (156)	0	0	0	0	0.25	0	1
1,798 Controls							
All genes (19,347)	6	6	12	12	-	-	-
Mouse hydrocephalus genes (189)	0	0	0	0	0.21	0	1
Dystroglycanopathies (12)	0	0	0	0	$8.1x10^{-3}$	0	1
Ciliopathies genes (22)	0	0	0	0	0.05	0	1
Cell adhesion molecules (142)	0	0	0	0	0.08	0	1
Wnt signaling pathway (156)	0	0	0	0	0.11	0	1

Supplementary Table 10. Damaging recessive genotypes in the mouse hydrocephalus and dystroglycanopathies gene sets are more enriched in 32 consanguineous cases compared to 341 non-consanguineous cases.

Gene Set (# genes)	Observed				Expected	Enrichment	P-value
	Homozygous	Compound heterozygous	Unique genes	Recessive genotypes	Recessive genotypes		
32 Consanguineous Cases							
All genes (19,347)	50	1	51	51	-	-	-
Mouse hydrocephalus genes (189)	5	0	5	5	0.89	5.63	$1.9x10^{-3}$
Dystroglycanopathies (12)	2	0	2	2	0.05	37.02	$1.4x10^{-3}$
Ciliopathies genes (22)	1	0	1	1	0.16	6.14	0.15
Cell adhesion molecules (142)	1	0	1	1	0.41	2.43	0.34
Wnt signaling pathway (156)	1	0	1	1	0.69	1.45	0.5
341 Non-Consanguineous Cases							
All genes (19,347)	19	20	38	39	-	-	-
Mouse hydrocephalus genes (189)	1	0	1	1	0.58	1.72	0.44
Dystroglycanopathies (12)	1	0	1	1	0.03	35.26	0.03
Ciliopathies genes (22)	0	0	0	0	0.12	0	1
Cell adhesion molecules (142)	0	0	0	0	0.27	0	1
Wnt signaling pathway (156)	0	0	0	0	0.43	0	1

Supplementary Table 11. Developmental phenotypes in mice and zebrafish with depletion of high-confidence hydrocephalus genes

Gene	Mouse Phenotypes	References	Zebrafish Phenotypes	References
TRIM71	Failure of cranial neural tube closure, exencephaly, embryonic lethality	PMIDs: 25883935, 19098426	Delayed and abnormal embryonic development	PMID: 17890240
SMARCC1	Exencephaly, abnormal embryonic neuroepithelial differentiation, failure in neural fold elevation, embryonic lethality	PMID: 11604513	Heterozygous post-fetal lethality	PMID: 28753627
PIK3CA	Abnormal brain vasculature morphology, growth retardation, embryonic lethality	PMIDs: 15687236, 18449193, 10196176	Decreased branchiness of retinal ganglion cell axon, collateral sprouting of retinal ganglion cell	PMID: 24218155
PTEN	Hydrocephalus, megacephaly, enlarged cerebrum, cerebellum and hippocampus (some cases), enlarged subependymal zone, increased amount of neuronal precursor cells, embryonic lethality	PMIDs: 11726926, 27815386, 16675393, 19470613, 12091320, 19211894, 9799734	abnormal hindbrain oligodendrocytes development	PMID: 27445141
MTOR	Absent embryonic telencephalon, buckling of the neuroepithelium in the forebrain, constrictions between the rostral and caudal diencephalon, growth retardation, embryonic lethality	PMIDs: 10079223, 11707573, 20008564, 15485918, 22193387	Delayed embryo development, decreased neuron myelination	PMIDs: 26538655, 30399334
FOXJ1	Hydrocephalus, absent ependyma motile cilia, absent subventricular zone cilia, growth retardation, post-fetal lethality	PMIDs: 9739041, 19906869, 10873152, 16325766, 21745638	Hydrocephalus, delayed embryo development, arrested epithelial cilium movement in extracellular fluid movement, immobile central canal motile cilium	PMIDs: 19284996, 20937855
FMN2	No neurodevelopmental phenotypes implicated		No neurodevelopmental phenotypes implicated	
PTCH1	Neural tube defect, exencephaly, abnormal telencephalon development, absent forebrain, increased medulloblastoma incidence, embryonic lethality	PMIDs: 9585239, 15576403, 9262482, 19321799, 12872247, 12361967, 21305688, 12386820, 21351254	Increased amount of neuronal stem cell in ciliary marginal zone, embryonic lethality	PMIDs: 19840373, 16121254
FXYD2	No neurodevelopmental phenotypes implicated		No neurodevelopmental phenotypes implicated	

Supplementary Table 12. Enrichment of overlapping genes with LoF or damaging *de novo* mutations between CH and Autism cohorts

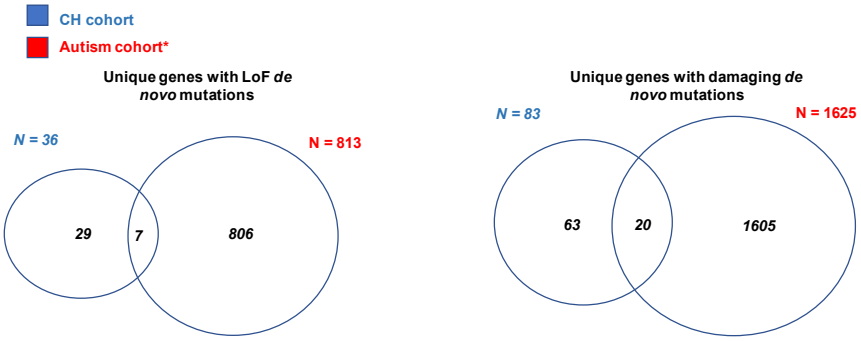

	Observed # genes	Expected # genes	Enrichment	Empirical P-value
Genes with LoF *de novo* mutations overlapping between CH and Autism cohorts	7	2.72	2.57	0.0164
Genes with damaging *de novo* mutations overlapping between CH and Autism cohorts	20	13.77	1.45	0.0494

10^6 permutations were performed to estimate the empirical distribution of the number of overlapping genes between CH and Autism cohorts. The empirical p-value is calculated as the proportion of the expected number of overlapping genes that exceeds the observed number of overlapping genes. For the detailed approach, please see **Online Methods**.*The Autism cohort refers to: (1) Satterstrom 2020 (10.1016/j.cell.2019.12.036)

Supplementary Table 13. Enrichment of overlapping genes with LoF or damaging *de novo* mutations between CH and DD cohorts

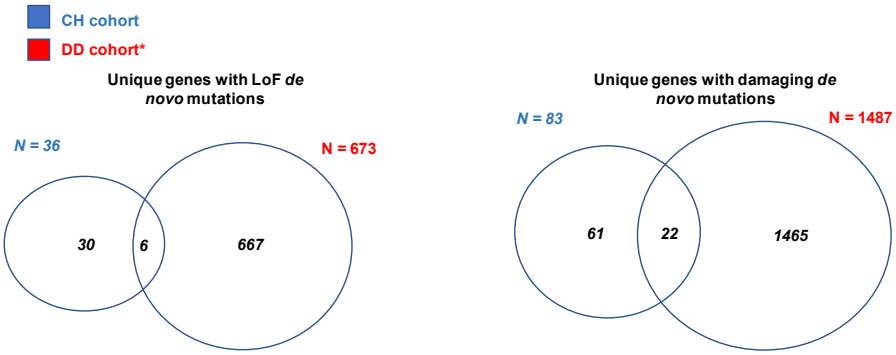

	Observed # genes	Expected # genes	Enrichment	Empirical P-value
Genes with LoF *de novo* mutations overlapping between CH and DD cohorts	6	2.3	2.61	0.0253
Genes with damaging *de novo* mutations overlapping between CH and DDD cohorts	22	13.12	1.68	0.0083

10^6 permutations were performed to estimate the empirical distribution of the number of overlapping genes between CH and DD cohorts. The empirical p-value is calculated as the proportion of the expected number of overlapping genes that exceeds the observed number of overlapping genes. For the detailed approach, please see **Methods**.*The DD cohort refers to: (1) DDD 2017 (10.1038/nature21062)

X. References

1. Kahle KT, Kulkarni AV, Limbrick DD, Jr., Warf BC. Hydrocephalus in children. Lancet (London, England) 2016;387:788-99.
2. Tully HM, Dobyns WB. Infantile hydrocephalus: a review of epidemiology, classification and causes. European journal of medical genetics 2014;57:359-68.
3. Simon TD, Riva-Cambrin J, Srivastava R, Bratton SL, Dean JM, Kestle JR. Hospital care for children with hydrocephalus in the United States: utilization, charges, comorbidities, and deaths. Journal of neurosurgery Pediatrics 2008;1:131-7.
4. Rekate HL. The definition and classification of hydrocephalus: a personal recommendation to stimulate debate. Cerebrospinal fluid research 2008;5:2.
5. Furey CG, Zeng X, Dong W, et al. Human Genetics and Molecular Mechanisms of Congenital Hydrocephalus. World neurosurgery 2018;119:441-3.
6. Jin SC, Dong W, Kundishora AJ, et al. Exome sequencing implicates genetic disruption of prenatal neuro-gliogenesis in sporadic congenital hydrocephalus. Nature medicine 2020.
7. Kousi M, Katsanis N. The Genetic Basis of Hydrocephalus. Annual review of neuroscience 2016;39:409-35.
8. Karimy JK, Reeves BC, Damisah E, et al. Inflammation in acquired hydrocephalus: pathogenic mechanisms and therapeutic targets. Nat Rev Neurol 2020.
9. Karimy JK, Duran D, Hu JK, et al. Cerebrospinal fluid hypersecretion in pediatric hydrocephalus. Neurosurg Focus 2016;41:E10.
10. Karimy JK, Zhang J, Kurland DB, et al. Inflammation-dependent cerebrospinal fluid hypersecretion by the choroid plexus epithelium in posthemorrhagic hydrocephalus. Nature medicine 2017;23:997-1003.
11. Dewan MC, Rattani A, Mekary R, et al. Global hydrocephalus epidemiology and incidence: systematic review and meta-analysis. Journal of neurosurgery 2018:1-15.
12. Stone SS, Warf BC. Combined endoscopic third ventriculostomy and choroid plexus cauterization as primary treatment for infant hydrocephalus: a prospective North American series. Journal of neurosurgery Pediatrics 2014;14:439-46.
13. Kulkarni AV, Riva-Cambrin J, Butler J, et al. Outcomes of CSF shunting in children: comparison of Hydrocephalus Clinical Research Network cohort with historical controls: clinical article. Journal of neurosurgery Pediatrics 2013;12:334-8.
14. Rodriguez EM, Guerra MM. Neural Stem Cells and Fetal-Onset Hydrocephalus. Pediatric neurosurgery 2017;52:446-61.
15. Fame RM, Cortes-Campos C, Sive HL. Brain Ventricular System and Cerebrospinal Fluid Development and Function: Light at the End of the Tube: A Primer with Latest Insights. Bioessays 2020;42:e1900186.
16. Saunders NR, Liddelow SA, Dziegielewska KM. Barrier mechanisms in the developing brain. Front Pharmacol 2012;3:46.
17. Gutzman JH, Sive H. Epithelial relaxation mediated by the myosin phosphatase regulator Mypt1 is required for brain ventricle lumen expansion and hindbrain morphogenesis. Development (Cambridge, England) 2010;137:795-804.
18. Brazel CY, Romanko MJ, Rothstein RP, Levison SW. Roles of the mammalian subventricular zone in brain development. Prog Neurobiol 2003;69:49-69.

19. Götz M, Huttner WB. The cell biology of neurogenesis. Nature reviews Molecular cell biology 2005;6:777-88.
20. Merkle FT, Alvarez-Buylla A. Neural stem cells in mammalian development. Current opinion in cell biology 2006;18:704-9.
21. Malatesta P, Appolloni I, Calzolari F. Radial glia and neural stem cells. Cell and tissue research 2008;331:165-78.
22. Sidman RL, Rakic P. Neuronal migration, with special reference to developing human brain: a review. Brain research 1973;62:1-35.
23. Weiss P. Anat Rec 1934;58.
24. Pollay M, Curl F. Secretion of cerebrospinal fluid by the ventricular ependyma of the rabbit. Am J Physiol 1967;213:1031-8.
25. Lowery LA, Sive H. Initial formation of zebrafish brain ventricles occurs independently of circulation and requires the nagie oko and snakehead/atp1a1a.1 gene products. Development (Cambridge, England) 2005;132:2057-67.
26. Bayer SA, Altman J. The human brain during the early first trimester: CRC Press; 2007.
27. Brinker T, Stopa E, Morrison J, Klinge P. A new look at cerebrospinal fluid circulation. Fluids and barriers of the CNS 2014;11:10.
28. Fame RM, Lehtinen MK. Emergence and Developmental Roles of the Cerebrospinal Fluid System. Developmental cell 2020;52:261-75.
29. Lehtinen MK, Bjornsson CS, Dymecki SM, Gilbertson RJ, Holtzman DM, Monuki ES. The choroid plexus and cerebrospinal fluid: emerging roles in development, disease, and therapy. The Journal of neuroscience : the official journal of the Society for Neuroscience 2013;33:17553-9.
30. Damkier HH, Brown PD, Praetorius J. Cerebrospinal fluid secretion by the choroid plexus. Physiol Rev 2013;93:1847-92.
31. Orešković D, Radoš M, Klarica M. Role of choroid plexus in cerebrospinal fluid hydrodynamics. Neuroscience 2017;354:69-87.
32. Bueno D, Parvas M, Garcia-Fernàndez J. The embryonic blood-cerebrospinal fluid barrier function before the formation of the fetal choroid plexus: role in cerebrospinal fluid formation and homeostasis. Croat Med J 2014;55:306-16.
33. Brown PD, Davies SL, Speake T, Millar ID. Molecular mechanisms of cerebrospinal fluid production. Neuroscience 2004;129:957-70.
34. Karimy JK, Kahle KT, Kurland DB, Yu E, Gerzanich V, Simard JM. A novel method to study cerebrospinal fluid dynamics in rats. J Neurosci Methods 2015;241:78-84.
35. Wu Q, Delpire E, Hebert SC, Strange K. Functional demonstration of Na+-K+-2Cl- cotransporter activity in isolated, polarized choroid plexus cells. Am J Physiol 1998;275:C1565-72.
36. Filippidis AS, Kalani MY, Rekate HL. Hydrocephalus and aquaporins: lessons learned from the bench. Child's nervous system : ChNS : official journal of the International Society for Pediatric Neurosurgery 2011;27:27-33.
37. MacAulay N, Zeuthen T. Water transport between CNS compartments: contributions of aquaporins and cotransporters. Neuroscience 2010;168:941-56.
38. Carter CS, Vogel TW, Zhang Q, et al. Abnormal development of NG2+PDGFR-alpha+ neural progenitor cells leads to neonatal hydrocephalus in a ciliopathy mouse model. Nature medicine 2012;18:1797-804.

39. Lancaster MA, Schroth J, Gleeson JG. Subcellular spatial regulation of canonical Wnt signalling at the primary cilium. Nature cell biology 2011;13:700-7.
40. Ocbina PJ, Eggenschwiler JT, Moskowitz I, Anderson KV. Complex interactions between genes controlling trafficking in primary cilia. Nature genetics 2011;43:547-53.
41. Zhang Q, Seo S, Bugge K, Stone EM, Sheffield VC. BBS proteins interact genetically with the IFT pathway to influence SHH-related phenotypes. Human molecular genetics 2012;21:1945-53.
42. Schneider C, Ramaswamy V, Kulkarni AV, et al. Clinical implications of medulloblastoma subgroups: incidence of CSF diversion surgery. Journal of neurosurgery Pediatrics 2015;15:236-42.
43. Ohata S, Herranz-Perez V, Nakatani J, Boletta A, Garcia-Verdugo JM, Alvarez-Buylla A. Mechanosensory Genes Pkd1 and Pkd2 Contribute to the Planar Polarization of Brain Ventricular Epithelium. The Journal of neuroscience : the official journal of the Society for Neuroscience 2015;35:11153-68.
44. Olstad EW, Ringers C, Hansen JN, et al. Ciliary Beating Compartmentalizes Cerebrospinal Fluid Flow in the Brain and Regulates Ventricular Development. Current biology : CB 2019;29:229-41.e6.
45. Fame RM, Chang JT, Hong A, Aponte-Santiago NA, Sive H. Directional cerebrospinal fluid movement between brain ventricles in larval zebrafish. Fluids and barriers of the CNS 2016;13:11.
46. Dandy WE. EXPERIMENTAL HYDROCEPHALUS. Ann Surg 1919;70:129-42.
47. Bateman GA, Brown KM. The measurement of CSF flow through the aqueduct in normal and hydrocephalic children: from where does it come, to where does it go? Child's nervous system : ChNS : official journal of the International Society for Pediatric Neurosurgery 2012;28:55-63.
48. Oi S, Di Rocco C. Proposal of "evolution theory in cerebrospinal fluid dynamics" and minor pathway hydrocephalus in developing immature brain. Child's nervous system : ChNS : official journal of the International Society for Pediatric Neurosurgery 2006;22:662-9.
49. Milhorat TH. Choroid plexus and cerebrospinal fluid production. Science (New York, NY) 1969;166:1514-6.
50. Krishnamurthy S, Li J, Schultz L, McAllister JP, 2nd. Intraventricular infusion of hyperosmolar dextran induces hydrocephalus: a novel animal model of hydrocephalus. Cerebrospinal fluid research 2009;6:16.
51. Di Rocco C, Pettorossi VE, Caldarelli M, Mancinelli R, Velardi F. Communicating hydrocephalus induced by mechanically increased amplitude of the intraventricular cerebrospinal fluid pressure: experimental studies. Experimental neurology 1978;59:40-52.
52. Wagshul ME, Eide PK, Madsen JR. The pulsating brain: A review of experimental and clinical studies of intracranial pulsatility. Fluids and barriers of the CNS 2011;8:5.
53. Wagshul ME, McAllister JP, Rashid S, et al. Ventricular dilation and elevated aqueductal pulsations in a new experimental model of communicating hydrocephalus. Experimental neurology 2009;218:33-40.
54. Greitz D. Paradigm shift in hydrocephalus research in legacy of Dandy's pioneering work: rationale for third ventriculostomy in communicating hydrocephalus. Child's

nervous system : ChNS : official journal of the International Society for Pediatric Neurosurgery 2007;23:487-9.
55. Iliff JJ, Wang M, Liao Y, et al. A paravascular pathway facilitates CSF flow through the brain parenchyma and the clearance of interstitial solutes, including amyloid β. Science translational medicine 2012;4:147ra11.
56. Qvarlander S, Lundkvist B, Koskinen LO, Malm J, Eklund A. Pulsatility in CSF dynamics: pathophysiology of idiopathic normal pressure hydrocephalus. J Neurol Neurosurg Psychiatry 2013;84:735-41.
57. Garne E, Loane M, Addor MC, Boyd PA, Barisic I, Dolk H. Congenital hydrocephalus--prevalence, prenatal diagnosis and outcome of pregnancy in four European regions. European journal of paediatric neurology : EJPN : official journal of the European Paediatric Neurology Society 2010;14:150-5.
58. Yamasaki M, Nonaka M, Suzumori N, et al. Prenatal molecular diagnosis of a severe type of L1 syndrome (X-linked hydrocephalus). Journal of neurosurgery Pediatrics 2011;8:411-6.
59. Quencer RM. Intracranial CSF flow in pediatric hydrocephalus: evaluation with cine-MR imaging. AJNR American journal of neuroradiology 1992;13:601-8.
60. Anik I, Etus V, Anik Y, Ceylan S. Role of interpeduncular and prepontine cistern cerebrospinal fluid flow measurements in prediction of endoscopic third ventriculostomy success in pediatric triventricular hydrocephalus. Pediatric neurosurgery 2010;46:344-50.
61. Faggin R, Calderone M, Denaro L, Meneghini L, d'Avella D. Long-term operative failure of endoscopic third ventriculostomy in pediatric patients: the role of cine phase-contrast MR imaging. Neurosurg Focus 2011;30:E1.
62. Jones RF, Stening WA, Brydon M. Endoscopic third ventriculostomy. Neurosurgery 1990;26:86-91; discussion -2.
63. Kulkarni AV, Drake JM, Mallucci CL, Sgouros S, Roth J, Constantini S. Endoscopic third ventriculostomy in the treatment of childhood hydrocephalus. The Journal of pediatrics 2009;155:254-9.e1.
64. Warf BC. Comparison of endoscopic third ventriculostomy alone and combined with choroid plexus cauterization in infants younger than 1 year of age: a prospective study in 550 African children. Journal of neurosurgery 2005;103:475-81.
65. Warf BC. Congenital idiopathic hydrocephalus of infancy: the results of treatment by endoscopic third ventriculostomy with or without choroid plexus cauterization and suggestions for how it works. Child's nervous system : ChNS : official journal of the International Society for Pediatric Neurosurgery 2013;29:935-40.
66. Warf BC, Tracy S, Mugamba J. Long-term outcome for endoscopic third ventriculostomy alone or in combination with choroid plexus cauterization for congenital aqueductal stenosis in African infants. Journal of neurosurgery Pediatrics 2012;10:108-11.
67. Warf BC, Dewan M, Mugamba J. Management of Dandy-Walker complex-associated infant hydrocephalus by combined endoscopic third ventriculostomy and choroid plexus cauterization. Journal of neurosurgery Pediatrics 2011;8:377-83.
68. Warf BC. Hydrocephalus associated with neural tube defects: characteristics, management, and outcome in sub-Saharan Africa. Child's nervous system : ChNS : official journal of the International Society for Pediatric Neurosurgery 2011;27:1589-94.

69. Smith ER, Butler WE, Barker FG, 2nd. In-hospital mortality rates after ventriculoperitoneal shunt procedures in the United States, 1998 to 2000: relation to hospital and surgeon volume of care. Journal of neurosurgery 2004;100:90-7.
70. Vinchon M, Baroncini M, Delestret I. Adult outcome of pediatric hydrocephalus. Child's nervous system : ChNS : official journal of the International Society for Pediatric Neurosurgery 2012;28:847-54.
71. Kandasamy J, Dwan K, Hartley JC, et al. Antibiotic-impregnated ventriculoperitoneal shunts--a multi-centre British paediatric neurosurgery group (BPNG) study using historical controls. Child's nervous system : ChNS : official journal of the International Society for Pediatric Neurosurgery 2011;27:575-81.
72. Kestle JR, Riva-Cambrin J, Wellons JC, 3rd, et al. A standardized protocol to reduce cerebrospinal fluid shunt infection: the Hydrocephalus Clinical Research Network Quality Improvement Initiative. Journal of neurosurgery Pediatrics 2011;8:22-9.
73. Kulkarni AV, Drake JM, Lamberti-Pasculli M. Cerebrospinal fluid shunt infection: a prospective study of risk factors. Journal of neurosurgery 2001;94:195-201.
74. Kariyattil R, Steinbok P, Singhal A, Cochrane DD. Ascites and abdominal pseudocysts following ventriculoperitoneal shunt surgery: variations of the same theme. Journal of neurosurgery 2007;106:350-3.
75. Ratilal B, Costa J, Sampaio C. Antibiotic prophylaxis for surgical introduction of intracranial ventricular shunts: a systematic review. Journal of neurosurgery Pediatrics 2008;1:48-56.
76. Rekate HL. Shunt-related headaches: the slit ventricle syndromes. Child's nervous system : ChNS : official journal of the International Society for Pediatric Neurosurgery 2008;24:423-30.
77. Kulkarni AV, Drake JM, Kestle JR, Mallucci CL, Sgouros S, Constantini S. Endoscopic third ventriculostomy vs cerebrospinal fluid shunt in the treatment of hydrocephalus in children: a propensity score-adjusted analysis. Neurosurgery 2010;67:588-93.
78. Durnford AJ, Kirkham FJ, Mathad N, Sparrow OC. Endoscopic third ventriculostomy in the treatment of childhood hydrocephalus: validation of a success score that predicts long-term outcome. Journal of neurosurgery Pediatrics 2011;8:489-93.
79. Sacko O, Boetto S, Lauwers-Cances V, Dupuy M, Roux FE. Endoscopic third ventriculostomy: outcome analysis in 368 procedures. Journal of neurosurgery Pediatrics 2010;5:68-74.
80. Drake JM. Endoscopic third ventriculostomy in pediatric patients: the Canadian experience. Neurosurgery 2007;60:881-6; discussion -6.
81. Bouras T, Sgouros S. Complications of endoscopic third ventriculostomy. World neurosurgery 2013;79:S22.e9-12.
82. Dalen K, Bruarøy S, Wentzel-Larsen T, Laegreid LM. Intelligence in children with hydrocephalus, aged 4-15 years: a population-based, controlled study. Neuropediatrics 2008;39:146-50.
83. Lacy M, Baldassarre M, Nader T, Frim D. Parent ratings of executive functioning in children with shunted hydrocephalus. Pediatric neurosurgery 2012;48:73-9.
84. Lacy M, Pyykkonen BA, Hunter SJ, et al. Intellectual functioning in children with early shunted posthemorrhagic hydrocephalus. Pediatric neurosurgery 2008;44:376-81.

85. Smith AD, Buckley MG. Spatial navigational impairments in hydrocephalus. Cogn Process 2012;13 Suppl 1:S329-32.
86. Lindquist B, Persson EK, Fernell E, Uvebrant P. Very long-term follow-up of cognitive function in adults treated in infancy for hydrocephalus. Child's nervous system : ChNS : official journal of the International Society for Pediatric Neurosurgery 2011;27:597-601.
87. Lindquist B, Persson EK, Uvebrant P, Carlsson G. Learning, memory and executive functions in children with hydrocephalus. Acta Paediatr 2008;97:596-601.
88. Kulkarni AV. Quality of life in childhood hydrocephalus: a review. Child's nervous system : ChNS : official journal of the International Society for Pediatric Neurosurgery 2010;26:737-43.
89. Persson EK, Hagberg G, Uvebrant P. Disabilities in children with hydrocephalus--a population-based study of children aged between four and twelve years. Neuropediatrics 2006;37:330-6.
90. Rekate HL, Kranz D. Headaches in patients with shunts. Semin Pediatr Neurol 2009;16:27-30.
91. Gupta N, Park J, Solomon C, Kranz DA, Wrensch M, Wu YW. Long-term outcomes in patients with treated childhood hydrocephalus. Journal of neurosurgery 2007;106:334-9.
92. McAllister JP, 2nd. Pathophysiology of congenital and neonatal hydrocephalus. Semin Fetal Neonatal Med 2012;17:285-94.
93. Schiff SJ, Ranjeva SL, Sauer TD, Warf BC. Rainfall drives hydrocephalus in East Africa. Journal of neurosurgery Pediatrics 2012;10:161-7.
94. Lattke M, Magnutzki A, Walther P, Wirth T, Baumann B. Nuclear factor κB activation impairs ependymal ciliogenesis and links neuroinflammation to hydrocephalus formation. The Journal of neuroscience : the official journal of the Society for Neuroscience 2012;32:11511-23.
95. Yung YC, Mutoh T, Lin ME, et al. Lysophosphatidic acid signaling may initiate fetal hydrocephalus. Science translational medicine 2011;3:99ra87.
96. Bateman GA, Smith RL, Siddique SH. Idiopathic hydrocephalus in children and idiopathic intracranial hypertension in adults: two manifestations of the same pathophysiological process? Journal of neurosurgery 2007;107:439-44.
97. Bateman GA. Hemodynamically significant venous collapse underlying neonatal hydrocephalus. Journal of neurosurgery Pediatrics 2014;13:125-32.
98. Ibrahim I, Rahme R, Hourani R, Ali Y, Melki I, Rizk T. Hydrocephalus following bilateral jugular venous thrombosis in a child: case report and review of the literature. Pediatric neurosurgery 2008;44:68-70.
99. Collmann H, Sörensen N, Krauss J. Hydrocephalus in craniosynostosis: a review. Child's nervous system : ChNS : official journal of the International Society for Pediatric Neurosurgery 2005;21:902-12.
100. Bateman G. Hyperemic hydrocephalus: a new form of childhood hydrocephalus analogous to hyperemic intracranial hypertension in adults. Journal of neurosurgery Pediatrics 2010;5:20-6.
101. Christensen IB, Gyldenholm T, Damkier HH, Praetorius J. Polarization of membrane associated proteins in the choroid plexus epithelium from normal and slc4a10 knockout mice. Front Physiol 2013;4:344.

102. Papadopoulos MC, Verkman AS. Potential utility of aquaporin modulators for therapy of brain disorders. Prog Brain Res 2008;170:589-601.
103. Poca MA, Sahuquillo J. Short-term medical management of hydrocephalus. Expert Opin Pharmacother 2005;6:1525-38.
104. Whitelaw A, Kennedy CR, Brion LP. Diuretic therapy for newborn infants with posthemorrhagic ventricular dilatation. Cochrane Database Syst Rev 2001:Cd002270.
105. Allocco AA, Jin SC, Duy PQ, et al. Recessive Inheritance of Congenital Hydrocephalus With Other Structural Brain Abnormalities Caused by Compound Heterozygous Mutations in ATP1A3. Frontiers in cellular neuroscience 2019;13:425.
106. Mao X, Enno TL, Del Bigio MR. Aquaporin 4 changes in rat brain with severe hydrocephalus. Eur J Neurosci 2006;23:2929-36.
107. Castañeyra-Ruiz L, González-Marrero I, González-Toledo JM, et al. Aquaporin-4 expression in the cerebrospinal fluid in congenital human hydrocephalus. Fluids and barriers of the CNS 2013;10:18.
108. Iliff JJ, Lee H, Yu M, et al. Brain-wide pathway for waste clearance captured by contrast-enhanced MRI. The Journal of clinical investigation 2013;123:1299-309.
109. Iliff JJ, Wang M, Zeppenfeld DM, et al. Cerebral arterial pulsation drives paravascular CSF-interstitial fluid exchange in the murine brain. The Journal of neuroscience : the official journal of the Society for Neuroscience 2013;33:18190-9.
110. Iliff JJ, Chen MJ, Plog BA, et al. Impairment of glymphatic pathway function promotes tau pathology after traumatic brain injury. The Journal of neuroscience : the official journal of the Society for Neuroscience 2014;34:16180-93.
111. Harris CA, McAllister JP, 2nd. What we should know about the cellular and tissue response causing catheter obstruction in the treatment of hydrocephalus. Neurosurgery 2012;70:1589-601; discussion 601-2.
112. Domínguez-Pinos MD, Páez P, Jiménez AJ, et al. Ependymal denudation and alterations of the subventricular zone occur in human fetuses with a moderate communicating hydrocephalus. Journal of neuropathology and experimental neurology 2005;64:595-604.
113. Young CC, van der Harg JM, Lewis NJ, Brooks KJ, Buchan AM, Szele FG. Ependymal ciliary dysfunction and reactive astrocytosis in a reorganized subventricular zone after stroke. Cerebral cortex (New York, NY : 1991) 2013;23:647-59.
114. Geschwind DH, Flint J. Genetics and genomics of psychiatric disease. Science (New York, NY) 2015;349:1489-94.
115. Polderman TJ, Benyamin B, de Leeuw CA, et al. Meta-analysis of the heritability of human traits based on fifty years of twin studies. Nature genetics 2015;47:702-9.
116. Munch TN, Rostgaard K, Rasmussen ML, Wohlfahrt J, Juhler M, Melbye M. Familial aggregation of congenital hydrocephalus in a nationwide cohort. Brain : a journal of neurology 2012;135:2409-15.
117. Munch TN, Rasmussen ML, Wohlfahrt J, Juhler M, Melbye M. Risk factors for congenital hydrocephalus: a nationwide, register-based, cohort study. J Neurol Neurosurg Psychiatry 2014;85:1253-9.
118. Warf BC. Hydrocephalus in Uganda: the predominance of infectious origin and primary management with endoscopic third ventriculostomy. Journal of neurosurgery 2005;102:1-15.

119. Adle-Biassette H, Saugier-Veber P, Fallet-Bianco C, et al. Neuropathological review of 138 cases genetically tested for X-linked hydrocephalus: evidence for closely related clinical entities of unknown molecular bases. Acta neuropathologica 2013;126:427-42.
120. Haverkamp F, Wölfle J, Aretz M, et al. Congenital hydrocephalus internus and aqueduct stenosis: aetiology and implications for genetic counselling. Eur J Pediatr 1999;158:474-8.
121. Lal D, Palotie A. Genetics Sheds New Light on Congenital Hydrocephalus Biology. Neuron 2018;99:246-7.
122. Sanders SJ, Murtha MT, Gupta AR, et al. De novo mutations revealed by whole-exome sequencing are strongly associated with autism. Nature 2012;485:237-41.
123. Ruzzo EK, Perez-Cano L, Jung JY, et al. Inherited and De Novo Genetic Risk for Autism Impacts Shared Networks. Cell 2019;178:850-66.e26.
124. Satterstrom FK, Kosmicki JA, Wang J, et al. Large-Scale Exome Sequencing Study Implicates Both Developmental and Functional Changes in the Neurobiology of Autism. Cell 2020.
125. Timberlake AT, Furey CG, Choi J, et al. De novo mutations in inhibitors of Wnt, BMP, and Ras/ERK signaling pathways in non-syndromic midline craniosynostosis. Proceedings of the National Academy of Sciences of the United States of America 2017;114:E7341-e7.
126. Allen AS, Berkovic SF, Cossette P, et al. De novo mutations in epileptic encephalopathies. Nature 2013;501:217-21.
127. Bilgüvar K, Oztürk AK, Louvi A, et al. Whole-exome sequencing identifies recessive WDR62 mutations in severe brain malformations. Nature 2010;467:207-10.
128. Prevalence and architecture of de novo mutations in developmental disorders. Nature 2017;542:433-8.
129. Willsey AJ, Morris MT, Wang S, et al. The Psychiatric Cell Map Initiative: A Convergent Systems Biological Approach to Illuminating Key Molecular Pathways in Neuropsychiatric Disorders. Cell 2018;174:505-20.
130. Kang HJ, Kawasawa YI, Cheng F, et al. Spatio-temporal transcriptome of the human brain. Nature 2011;478:483-9.
131. Willsey AJ, Sanders SJ, Li M, et al. Coexpression networks implicate human midfetal deep cortical projection neurons in the pathogenesis of autism. Cell 2013;155:997-1007.
132. Zhang B, Horvath S. A general framework for weighted gene co-expression network analysis. Stat Appl Genet Mol Biol 2005;4:Article17.
133. Parikshak NN, Luo R, Zhang A, et al. Integrative functional genomic analyses implicate specific molecular pathways and circuits in autism. Cell 2013;155:1008-21.
134. Nowakowski TJ, Bhaduri A, Pollen AA, et al. Spatiotemporal gene expression trajectories reveal developmental hierarchies of the human cortex. Science (New York, NY) 2017;358:1318-23.
135. Chong JX, Buckingham KJ, Jhangiani SN, et al. The Genetic Basis of Mendelian Phenotypes: Discoveries, Challenges, and Opportunities. Am J Hum Genet 2015;97:199-215.
136. Krumm N, Turner TN, Baker C, et al. Excess of rare, inherited truncating mutations in autism. Nature genetics 2015;47:582-8.

137. Furey CG, Choi J, Jin SC, et al. De Novo Mutation in Genes Regulating Neural Stem Cell Fate in Human Congenital Hydrocephalus. Neuron 2018;99:302-14.e4.
138. Duran D, Zeng X, Jin SC, et al. Mutations in Chromatin Modifier and Ephrin Signaling Genes in Vein of Galen Malformation. Neuron 2019;101:429-43.e4.
139. McKenna A, Hanna M, Banks E, et al. The Genome Analysis Toolkit: a MapReduce framework for analyzing next-generation DNA sequencing data. Genome Res 2010;20:1297-303.
140. Van der Auwera GA, Carneiro MO, Hartl C, et al. From FastQ data to high confidence variant calls: the Genome Analysis Toolkit best practices pipeline. Curr Protoc Bioinformatics 2013;43:11.0.1-.0.33.
141. Garrison E, Marth G. Haplotype-based variant detection from short-read sequencing. arXiv preprint arXiv:12073907 2012.
142. Wang K, Li M, Hakonarson H. ANNOVAR: functional annotation of genetic variants from high-throughput sequencing data. Nucleic Acids Res 2010;38:e164.
143. Karczewski KJ, Francioli LC, Tiao G, et al. The mutational constraint spectrum quantified from variation in 141,456 humans. Nature 2020;581:434-43.
144. Taliun D, Harris DN, Kessler MD, et al. Sequencing of 53,831 diverse genomes from the NHLBI TOPMed Program. BioRxiv 2019:563866.
145. Samocha KE, Kosmicki JA, Karczewski KJ, et al. Regional missense constraint improves variant deleteriousness prediction. BioRxiv 2017:148353.
146. Dong C, Wei P, Jian X, et al. Comparison and integration of deleteriousness prediction methods for nonsynonymous SNVs in whole exome sequencing studies. Human molecular genetics 2015;24:2125-37.
147. Wei Q, Zhan X, Zhong X, et al. A Bayesian framework for de novo mutation calling in parents-offspring trios. Bioinformatics 2015;31:1375-81.
148. Quinlan AR, Hall IM. BEDTools: a flexible suite of utilities for comparing genomic features. Bioinformatics 2010;26:841-2.
149. Samocha KE, Robinson EB, Sanders SJ, et al. A framework for the interpretation of de novo mutation in human disease. Nature genetics 2014;46:944-50.
150. Jin SC, Homsy J, Zaidi S, et al. Contribution of rare inherited and de novo variants in 2,871 congenital heart disease probands. Nature genetics 2017;49:1593-601.
151. Ware JS, Samocha KE, Homsy J, Daly MJ. Interpreting de novo Variation in Human Disease Using denovolyzeR. Curr Protoc Hum Genet 2015;87:7.25.1-7..15.
152. Wang M, Marco P, Capra V, Kibar Z. Update on the Role of the Non-Canonical Wnt/Planar Cell Polarity Pathway in Neural Tube Defects. Cells 2019;8.
153. Tissir F, Goffinet AM. Shaping the nervous system: role of the core planar cell polarity genes. Nat Rev Neurosci 2013;14:525-35.
154. Shaheen R, Sebai MA, Patel N, et al. The genetic landscape of familial congenital hydrocephalus. Annals of neurology 2017;81:890-7.
155. Walker RL, Ramaswami G, Hartl C, et al. Genetic Control of Expression and Splicing in Developing Human Brain Informs Disease Mechanisms. Cell 2019;179:750-71.e22.
156. Langfelder P, Horvath S. WGCNA: an R package for weighted correlation network analysis. BMC Bioinformatics 2008;9:559.
157. Li J, Zhou D, Qiu W, et al. Application of Weighted Gene Co-expression Network Analysis for Data from Paired Design. Scientific reports 2018;8:622.

158. Raudvere U, Kolberg L, Kuzmin I, et al. g:Profiler: a web server for functional enrichment analysis and conversions of gene lists (2019 update). Nucleic Acids Res 2019;47:W191-w8.
159. Polioudakis D, de la Torre-Ubieta L, Langerman J, et al. A Single-Cell Transcriptomic Atlas of Human Neocortical Development during Mid-gestation. Neuron 2019;103:785-801.e8.
160. Duy PQ, Furey CG, Kahle KT. Trim71/lin-41 Links an Ancient miRNA Pathway to Human Congenital Hydrocephalus. Trends Mol Med 2019;25:467-9.
161. Narayanan R, Pirouz M, Kerimoglu C, et al. Loss of BAF (mSWI/SNF) Complexes Causes Global Transcriptional and Chromatin State Changes in Forebrain Development. Cell reports 2015;13:1842-54.
162. Harmacek L, Watkins-Chow DE, Chen J, et al. A unique missense allele of BAF155, a core BAF chromatin remodeling complex protein, causes neural tube closure defects in mice. Dev Neurobiol 2014;74:483-97.
163. Liu P, Cheng H, Roberts TM, Zhao JJ. Targeting the phosphoinositide 3-kinase pathway in cancer. Nat Rev Drug Discov 2009;8:627-44.
164. Li L, Liu F, Ross AH. PTEN regulation of neural development and CNS stem cells. J Cell Biochem 2003;88:24-8.
165. Chalhoub N, Baker SJ. PTEN and the PI3-kinase pathway in cancer. Annu Rev Pathol 2009;4:127-50.
166. Keppler-Noreuil KM, Parker VE, Darling TN, Martinez-Agosto JA. Somatic overgrowth disorders of the PI3K/AKT/mTOR pathway & therapeutic strategies. Am J Med Genet C Semin Med Genet 2016;172:402-21.
167. Foerster P, Daclin M, Asm S, et al. mTORC1 signaling and primary cilia are required for brain ventricle morphogenesis. Development (Cambridge, England) 2017;144:201-10.
168. Groszer M, Erickson R, Scripture-Adams DD, et al. Negative regulation of neural stem/progenitor cell proliferation by the Pten tumor suppressor gene in vivo. Science (New York, NY) 2001;294:2186-9.
169. Jacquet BV, Salinas-Mondragon R, Liang H, et al. FoxJ1-dependent gene expression is required for differentiation of radial glia into ependymal cells and a subset of astrocytes in the postnatal brain. Development (Cambridge, England) 2009;136:4021-31.
170. Lian G, Chenn A, Ekuta V, Kanaujia S, Sheen V. Formin 2 Regulates Lysosomal Degradation of Wnt-Associated β-Catenin in Neural Progenitors. Cerebral cortex (New York, NY : 1991) 2019;29:1938-52.
171. Lian G, Dettenhofer M, Lu J, et al. Filamin A- and formin 2-dependent endocytosis regulates proliferation via the canonical Wnt pathway. Development (Cambridge, England) 2016;143:4509-20.
172. Gavino C, Richard S. Patched1 haploinsufficiency impairs ependymal cilia function of the quaking viable mice, leading to fatal hydrocephalus. Molecular and cellular neurosciences 2011;47:100-7.
173. Palma V, Lim DA, Dahmane N, et al. Sonic hedgehog controls stem cell behavior in the postnatal and adult brain. Development (Cambridge, England) 2005;132:335-44.
174. Palma V, Ruiz i Altaba A. Hedgehog-GLI signaling regulates the behavior of cells with stem cell properties in the developing neocortex. Development (Cambridge, England) 2004;131:337-45.

175. Divina P, Kvitkovicova A, Buratti E, Vorechovsky I. Ab initio prediction of mutation-induced cryptic splice-site activation and exon skipping. Eur J Hum Genet 2009;17:759-65.
176. Bult CJ, Blake JA, Smith CL, Kadin JA, Richardson JE. Mouse Genome Database (MGD) 2019. Nucleic Acids Res 2019;47:D801-d6.
177. Hehr U, Uyanik G, Gross C, et al. Novel POMGnT1 mutations define broader phenotypic spectrum of muscle-eye-brain disease. Neurogenetics 2007;8:279-88.
178. Manzini MC, Tambunan DE, Hill RS, et al. Exome sequencing and functional validation in zebrafish identify GTDC2 mutations as a cause of Walker-Warburg syndrome. Am J Hum Genet 2012;91:541-7.
179. Kurata H, Shirai K, Saito Y, et al. Neurodevelopmental disorders in children with macrocephaly: A prevalence study and PTEN gene analysis. Brain & development 2018;40:36-41.
180. Palmen SJ, Hulshoff Pol HE, Kemner C, et al. Increased gray-matter volume in medication-naive high-functioning children with autism spectrum disorder. Psychol Med 2005;35:561-70.
181. Gilmore JH, van Tol JJ, Lewis Streicher H, et al. Outcome in children with fetal mild ventriculomegaly: a case series. Schizophr Res 2001;48:219-26.
182. Iossifov I, O'Roak BJ, Sanders SJ, et al. The contribution of de novo coding mutations to autism spectrum disorder. Nature 2014;515:216-21.
183. O'Rourke DJ, Twomey E, Lynch SA, King MD. Cortical dysplasia associated with the PTEN mutation in Bannayan Riley Ruvalcaba syndrome: a rare finding. Clin Dysmorphol 2012;21:91-2.
184. Chen HH, Händel N, Ngeow J, et al. Immune dysregulation in patients with PTEN hamartoma tumor syndrome: Analysis of FOXP3 regulatory T cells. J Allergy Clin Immunol 2017;139:607-20.e15.
185. Sarquis MS, Agrawal S, Shen L, Pilarski R, Zhou XP, Eng C. Distinct expression profiles for PTEN transcript and its splice variants in Cowden syndrome and Bannayan-Riley-Ruvalcaba syndrome. Am J Hum Genet 2006;79:23-30.
186. Mirzaa GM, Campbell CD, Solovieff N, et al. Association of MTOR Mutations With Developmental Brain Disorders, Including Megalencephaly, Focal Cortical Dysplasia, and Pigmentary Mosaicism. JAMA neurology 2016;73:836-45.
187. Wallmeier J, Frank D, Shoemark A, et al. De Novo Mutations in FOXJ1 Result in a Motile Ciliopathy with Hydrocephalus and Randomization of Left/Right Body Asymmetry. Am J Hum Genet 2019;105:1030-9.
188. Guerra MM, Henzi R, Ortloff A, et al. Cell Junction Pathology of Neural Stem Cells Is Associated With Ventricular Zone Disruption, Hydrocephalus, and Abnormal Neurogenesis. Journal of neuropathology and experimental neurology 2015;74:653-71.
189. Wagner C, Batiz LF, Rodriguez S, et al. Cellular mechanisms involved in the stenosis and obliteration of the cerebral aqueduct of hyh mutant mice developing congenital hydrocephalus. Journal of neuropathology and experimental neurology 2003;62:1019-40.
190. Zega K, Jovanovic VM, Vitic Z, et al. Dusp16 Deficiency Causes Congenital Obstructive Hydrocephalus and Brain Overgrowth by Expansion of the Neural Progenitor Pool. Front Mol Neurosci 2017;10:372.

191. Henzi R, Vio K, Jara C, et al. Neural stem cell therapy of foetal onset hydrocephalus using the HTx rat as experimental model. Cell and tissue research 2020.
192. McAllister JP, Guerra MM, Ruiz LC, et al. Ventricular Zone Disruption in Human Neonates With Intraventricular Hemorrhage. Journal of neuropathology and experimental neurology 2017;76:358-75.
193. Lindquist B, Carlsson G, Persson EK, Uvebrant P. Behavioural problems and autism in children with hydrocephalus : a population-based study. Eur Child Adolesc Psychiatry 2006;15:214-9.
194. Movsas TZ, Pinto-Martin JA, Whitaker AH, et al. Autism spectrum disorder is associated with ventricular enlargement in a low birth weight population. The Journal of pediatrics 2013;163:73-8.
195. Li M, Santpere G, Imamura Kawasawa Y, et al. Integrative functional genomic analysis of human brain development and neuropsychiatric risks. Science (New York, NY) 2018;362.
196. Etchegaray A, Juarez-Peñalva S, Petracchi F, Igarzabal L. Prenatal genetic considerations in congenital ventriculomegaly and hydrocephalus. Child's nervous system : ChNS : official journal of the International Society for Pediatric Neurosurgery 2020;36:1645-60.